EUROPEAN RESPIRATORY journal
FLAGSHIP SCIENTIFIC JOURNAL OF ERS

Early View

Original research article

Pulmonary infection by SARS-CoV-2 induces senescence accompanied by an inflammatory phenotype in severe COVID-19: possible implications for viral mutagenesis

Konstantinos Evangelou, Dimitris Veroutis, Koralia Paschalaki, Periklis G. Foukas, Nefeli Lagopati, Marios Dimitriou, Angelos Papaspyropoulos, Bindu Konda, Orsalia Hazapis, Aikaterini Polyzou, Sophia Havaki, Athanassios Kotsinas, Christos Kittas, Athanasios G. Tzioufas, Laurence de Leval, Demetris Vassilakos, Sotirios Tsiodras, Barry R. Stripp, Argyris Papantonis, Giovanni Blandino, Ioannis Karakasiliotis, Peter J Barnes, Vassilis G. Gorgoulis

Please cite this article as: Evangelou K, Veroutis D, Paschalaki K, *et al*. Pulmonary infection by SARS-CoV-2 induces senescence accompanied by an inflammatory phenotype in severe COVID-19: possible implications for viral mutagenesis. *Eur Respir J* 2022; in press (https://doi.org/10.1183/13993003.02951-2021).

This manuscript has recently been accepted for publication in the *European Respiratory Journal*. It is published here in its accepted form prior to copyediting and typesetting by our production team. After these production processes are complete and the authors have approved the resulting proofs, the article will move to the latest issue of the ERJ online.

Pulmonary infection by SARS-CoV-2 induces senescence accompanied by an inflammatory phenotype in severe COVID-19: possible implications for viral mutagenesis

Konstantinos Evangelou[1*], Dimitris Veroutis[1*], Koralia Paschalaki[2*], Periklis G. Foukas[3], Nefeli Lagopati[1], Marios Dimitriou[4], Angelos Papaspyropoulos[1], Bindu Konda[5], Orsalia Hazapis[1], Aikaterini Polyzou[1], Sophia Havaki[1], Athanassios Kotsinas[1], Christos Kittas[1], Athanasios G. Tzioufas[6], Laurence de Leval[7], Demetris Vassilakos[1], Sotirios Tsiodras[8,9], Barry R. Stripp[5], Argyris Papantonis[10,11], Giovanni Blandino[12], Ioannis Karakasiliotis[4], Peter J Barnes[2#] and Vassilis G. Gorgoulis[1,13,14,15,16#]

1. Molecular Carcinogenesis Group, Department of Histology and Embryology, Medical School, National and Kapodistrian University of Athens, Athens, Greece
2. National Heart and Lung Institute, Imperial College London, London, UK
3. 2nd Department of Pathology, Attikon University Hospital, Medical School, National and Kapodistrian University of Athens, Athens, Greece
4. Laboratory of Biology, Department of Medicine, Democritus University of Thrace, Alexandroupolis, Greece
5. Lung and Regenerative Medicine Institutes, Cedars-Sinai Medical Center, Los Angeles, USA
6. Department of Pathophysiology, Medical School, National and Kapodistrian University of Athens, Athens, Greece
7. Institute of Pathology, Lausanne University Hospital, Lausanne, Switzerland.
8. 4th Department of Internal Medicine, Attikon University Hospital, University of Athens Medical School, Athens, Greece
9. Hellenic Centre for Disease Control and Prevention, Athens, Greece

10. Translational Epigenetics Group, Institute of Pathology, University Medical Center Göttingen, Göttingen, Germany
11. Center for Molecular Medicine, University of Cologne, Cologne, Germany
12. Oncogenomic and Epigenetic Unit, IRCCS, Regina Elena National Cancer Institute, Rome, Italy
13. Faculty Institute for Cancer Sciences, Manchester Academic Health Sciences Centre, University of Manchester, Manchester, UK
14. Biomedical Research Foundation, Academy of Athens, Athens, Greece
15. Center for New Biotechnologies and Precision Medicine, Medical School, National and Kapodistrian University of Athens, Athens, Greece
16. Faculty of Health and Medical Sciences, University of Surrey, UK

*** Contributed equally**

#Corresponding Authors:

Professor Vassilis G Gorgoulis MD, PhD
Department Histology-Embryology, Medical School, National Kapodistrian University of Athens, 75 Mikras Asias Str, Goudi, Athens GR11527, Greece
phone: +302107462352
email: vgorg@med.uoa.gr

Professor Peter J Barnes FRS, FMedSci
Airway Disease Section, National Heart & Lung Institute, Dovehouse St, London SW3 6LY, United Kingdom
phone: +44 20 7594 7959; fax: +44 20 7351 8126
email: p.j.barnes@imperial.ac.uk

Author contributions: K.E., D.V.: immunocytochemistry, SenTraGor^{TM} staining; K.E., P.G.F., C.K., L.DL, V.G.G.: histopathological examination and evaluation of the stainings; M.D., I.K.: cell culture and viral manipulations; B.S.: 3D alveosphere system and viral manipulations; A.K., An.P.: RNA and protein extraction, RT-qPCR, NGS, western blot; N.L., S.H.: electron microscopy; O.H., Ai.P.: Statistical analysis, bioinformatic analysis and graphs generation; D.Va.: anti-SARS-CoV-2 antibody generation; K.E., A.G.T, K.P., S.T., V.G.G.: data analysis and interpretation, manuscript preparation; S.T., Ar. P., G.B., P.J.B., V.G.G.: experimental design, guidance, manuscript writing with input for all co-authors.

Funding: This work was supported by the: National Public Investment Program of the Ministry of Development and Investment / General Secretariat for Research and Technology, in the framework of the Flagship Initiative to address SARS-CoV-2 (2020ΣΕ01300001); Horizon 2020 Marie Sklodowska-Curie training program no. 722729 (SYNTRAIN); Welfare Foundation for Social & Cultural Sciences, Athens, Greece (KIKPE); H. Pappas donation; Hellenic Foundation for Research and Innovation (HFRI) grants no. 775 and 3782 and NKUA-SARG grant 70/3/8916.

Short title: SARS-CoV-2 induces cellular senescence

Abstract

Background: SARS-CoV-2 infection of the respiratory system can progress to a multi-systemic disease with aberrant inflammatory response. Cellular senescence promotes chronic inflammation, named as senescence-associated secretory phenotype (SASP). We investigated whether COVID-19 disease is associated with cellular senescence and SASP.

Methods: Autopsy lung tissue samples from 11 COVID-19 patients and 43 age-matched non-COVID controls with similar comorbidities were analysed by immunohistochemistry for SARS-CoV-2, markers of senescence and key SASP cytokines. Virally-induced senescence was functionally recapitulated *in vitro*, by infecting epithelial Vero-E6 cells and a three-dimensional alveosphere system of alveolar type 2 (AT2) cells with SARS-CoV-2 strains isolated from COVID-19 patients.

Results: SARS-CoV-2 was detected by immunocytochemistry and electron microscopy predominantly in AT2 cells. Infected AT2 cells expressed the angiotensin-converting-enzyme 2 (ACE2) and exhibited increased senescence ($p16^{INK4A}$ and SenTraGor^{TM} positivity) and IL-1β and IL-6 expression. *In vitro*, infection of Vero-E6 cells with SARS-CoV-2 induced senescence (SenTraGor^{TM}), DNA damage (γ-H2AX) and increased cytokine (IL-1β, IL-6, CXCL8) and Apolipoprotein B mRNA-editing (APOBEC) enzyme expression. Next-generation-sequencing analysis of progenies obtained from infected/senescent Vero-E6 cells demonstrated APOBEC-mediated SARS-CoV-2 mutations. Dissemination of the SARS-CoV-2-infection and senescence was confirmed in extra-pulmonary sites (kidney and liver) of a COVID-19 patient.

Conclusions: We demonstrate that in severe COVID-19, AT2 cells infected by SARS-CoV-2 exhibit senescence and a proinflammatory phenotype. *In vitro*, SARS-CoV-2 infection induces senescence and inflammation. Importantly, infected senescent cells may act as a

source of SARS-CoV-2 mutagenesis mediated by APOBEC enzymes. Therefore, SARS-CoV-2-induced senescence may be an important molecular mechanism of severe COVID-19, disease persistence and mutagenesis.

Words: 250

Key words: SARS-CoV-2, COVID-19, cellular senescence, senescence-associated secretory phenotype (SASP), alveolar type-2 (AT2) cells, apolipoprotein B mRNA editing enzyme, catalytic polypeptide-like (APOBEC), mutations

Introduction

The severe acute respiratory syndrome coronavirus 2 (SARS-CoV-2) causes coronavirus disease 2019 (COVID-19) that primarily affects the respiratory system. The clinical course of the patients ranges from asymptomatic to a life-threatening respiratory failure accompanied by a multi-systemic inflammatory disease [1, 2]. Systemic disease may occur through a virally-mediated inflammatory response that consists of a variety of proinflammatory cytokines and chemokines, including interleukin (IL)-1β, IL-6, IL-12, IFN-γ, TNF-α, CXCL-8, CXCL-10 and CCL-2 [3, 4]. The link between viral infection of cells and development of severe lung disease and systemic manifestations is still poorly understood. Viral infection results in the activation of complex innate and adaptive immune responses that are orchestrated sequentially, involving several cell types and inflammatory mediators [5, 6]. At the cellular level, intrinsic defence mechanisms are activated and outcomes range from complete recovery to cell death [7-11]. An "intermediate" and essential cellular state that is overlooked, due to lack of efficient methodological tools, is cellular senescence [12, 13].

Cellular senescence is a stress response mechanism that preserves homeostasis. Senescent cells are characterized by prolonged and generally irreversible cell-cycle arrest and resistance to apoptosis [12, 14]. Additionally, they also exhibit secretory features, collectively described as the senescence-associated secretory phenotype (SASP) [12]. SASP includes a variety of cytokines, chemokines, growth factors, proteases and other molecules, depending on the type of senescence and the cells involved [12, 15]. These inflammatory proteins are released in the extracellular space as soluble factors, transmembrane proteins following ectodomain shedding, or as molecules engulfed within extracellular vesicles [16-18]. Cellular senescence plays a key role in several lung diseases, involving the senescence of several cell types in the lung [19, 20]. Under physiological conditions, senescence is

transiently activated and SASP mediates the recruitment of immune cells for senescent cell clearance. In addition, other SASP factors promote tissue regeneration and repair, overall ensuring cellular/tissue homeostasis. On the contrary, persistence of senescent cells exerts harmful properties promoting tissue dysfunction and the maintenance of chronic inflammation, via paracrine and systemic SASP [12, 15].

There is little published evidence linking viral infection to cellular senescence [21-26]. Given the implication of an inflammatory response in the progression of COVID-19 and the SASP secretion by senescent cells, we investigated whether cellular senescence occurs in COVID-19. Since individual markers are not adequate to unequivocally detect senescence, especially *in vivo*, as they may also be present in non senescent conditions, we followed in a clinical setting a detailed multi-marker algorithmic approach that we and others recently published and was approved by the senescence community [12, 27]. We were the first to provide evidence supporting the proof for senescence in COVID-19 infected lung tissue by applying this algorithm in a previous, preprint (bioRvix), version of the current manuscript [28], which subsequently has been confirmed by others [29]. This is the largest clinical study verifying viral-induced senescence by SARS-CoV-2 infection linked to a proinflammatory phenotype, which may contribute to acute and chronic clinical manifestations in severe COVID-19. Importantly, we also provide novel evidence for the generation of viral mutations promoted by SARS-CoV-2 persistence in senescent cells.

Materials and Methods

Tissues

Formalin-fixed and paraffin-embedded autopsy lung tissue samples were obtained from 11 patients that died from severe COVID-19 (confirmed by RT-qPCR) (**Table 1 and Table S1A**). Lung parenchyma displaying analogous lesions (atelectasia, fibrosis and infiltration by immune cells) from 43 age-matched patients with similar comorbidities from previously published cohort [30] and new cases, resected prior to the COVID-19 outbreak, were used for comparison with COVID-19 samples for all experiments detailed below (negative controls) (**Table 1 and Table S1B**). A non-COVID cohort of 60 age-matched lung samples was used as biological negative controls for validation of the anti-SARS-CoV-2 (G2) monoclonal antibody (online supplement). Moreover, renal and liver tissue from one of the eleven COVID-19 cases and five non-COVID-19 patients were also available and analysed for the presence of the virus and cellular senescence. Clinical sample collection and their experimental use were approved by the Commission Cantonale D'éthique de la Recherche, University of Lausanne, Switzerland (2020-01257) and the Bio-Ethics Committee of the University of Athens Medical School, Greece.

Cells and SARS-CoV-2 culture

SARS-CoV-2 (isolate 30-287, B.1.222 and B.1 strain (accession No MT459880.1) was obtained through culture in Vero E6 cells (ATCC® CRL-1586), from two different infected (COVID-19) patients. The virus was recovered from a nasopharyngeal swab, rinsed in 1 ml saline and filtered twice through a 0.22 nm filter. Virus stock was prepared by infecting fully confluent

Vero-E6 cells in DMEM, 10% fetal bovine serum (FBS) with antibiotics, at 37^{o}C and 5% CO_2. Virus stock was collected four days after inoculation, sequenced by NGS (online supplement) and the supernatant was frozen (−80°C) until use. Infections were carried out in 24-well plates, using SARS-CoV-2 at a 0.01 MOI. Cells were either fixed with 4% paraformaldehyde or lysed with NucleoZOL (Macherey-Nagel) 17 days post infection. Administration of the specific ataxia-telangiectasia-mutated (ATM) protein kinase inhibitor KU-55933 was carried out as described elsewhere [31]. Three independent experiments were performed. All manipulations were carried out in a Biosafety level 3 facility.

SARS-CoV-2 primary human lung alveosphere system

Formalin fixed and paraffin embedded sections from a three-dimensional alveosphere system infected with SARS-CoV-2 and corresponding controls (non-infected) were analysed. The alveospheres consist of self-renewing AT2 cells that express the well-established AT2 cell markers, HTII-280 and surfactant protein C as well as of some cells expressing the AT1 cell marker HTI 56 [32]. Alveospheres were gently opened using pipetting to allow infection and to avoid cellular stress [32].

Anti-SARS-COV-2 (G2) antibody generation

Mouse immunization and antibody collection, selection and specificity determination are described in the online supplement. Transcriptome analysis of hybridomas and amino acid determination of selected clones are also provided. Four clones, (479-S1, 480-S2, 481-S3 and 482-S4) are under patent application (Gorgoulis VG, Vassilakos D, Kastrinakis N. GR-patent application no: 22-0003846810).

RNA extraction and Reverse-Transcription real-time PCR (RT-qPCR) detection were performed as previously described (online supplement) [33].

Next Generation Sequencing (NGS)

NGS was performed as previously described (online supplement)[34].

Protein extraction and immunoblot analysis

Protein extraction and immunoblot analysis was performed as described elsewhere [31]. For details see online supplement. Horse Radish Peroxidase conjugated anti-goat, anti-mouse and anti-rabbit secondary antibodies (1:1000 dilution) (Cell Signaling) were used. Primary antibodies were: anti-APOBEC (apolipoprotein B mRNA editing enzyme, catalytic polypeptide-like) 3G/A3G (Abcam ab109727 and ab172694), anti‑APOBEC3H (LSBio LS‑C151868) and anti-GAPDH (Cell Signaling).

Immunocytochemistry and Immunohistochemistry

Immunocytochemistry and immunohistochemistry were performed according to published protocols [34]. The following primary antibodies were applied overnight at 4^{o}C: anti-SARS-CoV-2 (G2) monoclonal antibody (at a dilution 1:300), anti-SARS-CoV-2 monoclonal antibody (1A9 clone, Genetek), anti-ACE-2 (Abcam), anti-thyroid transcription factor (TTF)-1 (Dako), anti-Surfactant Protein B (SP-B) (1B9 clone, ZETA Corporation), anti-$p16^{INK4A}$ (Santa Cruz), anti-IL-1β (Abcam), anti-IL-6 (R&D systems), anti-phospho-histone (Ser^{139}) H2AX (γH2AX) (Cell Signaling), anti-Ki67 (Abcam) and anti-$p21^{Waf1/Cip1}$(Cell Signaling).

Senescence-SenTraGor^{TM} (GL13) methodology

SenTraGor™ (trademark of GL13 compound) staining and double staining experiments were performed and evaluated as previously described [27, 35]. The mean percentage of SenTraGor positive alveolar cells in at least 10 high power fields (x400) per patient was quantified.

Electron microscopy

Representative area from hematoxylin and eosin-stained paraffin sections of the lung autopsy of COVID-19 patients and non COVID-19 controls were chosen under the light microscope and marked. Paraffin-embedded tissue was deparaffinized, rehydrated and fixed in 2.5% glutaraldehyde in PBS for 24h and post-fixed in 1% aqueous osmium.

Bioinformatic analysis for identification of mutational signatures in the SARS-CoV-2 genome

As described in detail in online supplement, candidacy for APOBEC deamination of C→U mutational substitutions in the SARS-CoV-2 genome of strains available in GISAID database [36, 37] and in those obtained after cell culture infection, was examined and verified against experimentally validated APOBEC motifs (**Figure S7)**.

Statistical analysis

Data are expressed as mean ± SD. Comparisons were performed with unpaired non-parametric Mann-Whitney U test (comparison between two groups) or Kruskal Wallis test followed by Dunn's post-hoc analysis (comparison between three groups). The Wilcoxon paired non-parametric test was used to compare values of infected cells *in vitro*.

Results

Detection of SARS-CoV-2 in lung cells

In order to detect SARS-CoV-2 in lung tissue we developed monoclonal antibodies which react against receptor-binding domain (RBD) of the spike protein of SARS-CoV-2 and identified a high affinity antibody (G2), the validity of which was recently verified [38] (**Figure S1, Table S1)**. SARS-CoV-2 was detected (using both our 'in house' G2 clone and a commercially available antibody from GeneTek) predominantly in alveolar type 2 (AT2) cells, which were identified by TTF-1 and Surfactant Protein B (SP-B) positivity, and in sparse inflammatory cells (alveolar and tissue macrophages) in all COVID-19 patients, ranging from <5 cells/4mm^2 tissue to >50 cells/4mm^2 tissue (**Figure 1A, Table S1A**). Surface epithelial cells in small peripheral airways stained also positive in certain cases (**Figure S2**). SARS-CoV-2 infected AT2 cells were occasionally large and appeared isolated (denuded or syncytial) or clustered (hyperplasia), exhibiting a variety of topological distribution (**Figure 1A**). These cells co-expressed the angiotensin-converting enzyme 2 (ACE2) receptor (**Figure 1B**), supporting SARS-CoV-2 infection being mediated by the ACE2 receptor [39]. In addition, electron microscopy analysis in representative COVID-19 cases confirmed the presence of virus within AT2 cells (**Figure 1C**) and high magnification revealed virions in the proximity of the endoplasmic reticulum, indicating their likely assembly and budding, as well as virions residing in cytoplasmic vesicles, implying their transfer and release into the extracellular space.

Senescence in SARS-CoV-2 infected cells

A proportion of SARS-CoV-2 infected AT2 cells (range 8-21%) displayed a senescent phenotype, with positive staining for SenTraGor^{TM} and p16^{INK4A} (**Figure 2A-C, Figure S3**)

[12,29,30]. SenTraGor™ is an established marker of senescence and has the unique property of detecting senescent cells in any setting, including archival material [formalin-fixed paraffin embedded (FFPE) tissue)] [12, 27, 35]. By contrast, lung tissues exhibiting fibrosis, atelectasia and inflammatory infiltrates from age-matched non-COVID-19 cases with similar co-morbidities (**Table 1 and Table S1**), including a separate control cohort of patients with acute pneumonia (aspiration pneumonia), showed significantly lower senescence (range 1-2%, $p<0.0001$) (**Figure 2A-C, Figure S4**), suggesting that SARS-CoV-2 infection may induce senescence.

In order to demonstrate that SARS-CoV-2 can induce cellular senescence, we infected Vero cells with a viral strain isolated from a COVID-19 patient. Vero-E6 cells is an established cellular system for viral propagation and studies, as apart from their high infectivity to SARS-CoV-2 they are among the few cell lines demonstrating SARS-CoV-2-mediated cytopathic effects, an essential aspect in diagnostics [40, 41]. Infection was carried out at a low multiplicity of infection (MOI) to mimic natural coronavirus infection [42]. In line with our hypothesis, the infected cells following an initial surge of cell death reached an equilibrium demonstrating clear evidence of senescence (increased SenTraGor positivity, increased $p21^{WAF1/CIP1}$ and reduced Ki-67), as compared to the non-infected control cells at 17 days post infection (**Figure 3 and S5A**). As Vero cells lack $p16^{INK4A}$ [43], the most likely trigger of senescence is DNA damage, as previously reported [12, 13]. DNA damage measured by γ-H2AX immunostaining was evident in SARS-CoV-2 infected cells (**Figure 3A4**). Treatment of infected cells with a selective ATM inhibitor (KU-55933) dramatically decreased senescence assessed by SenTraGor staining (**Figure S6**). ATM has been previously reported as a key driver of NF-κB-dependent DNA-damage-induced senescence [44]. It appears that genotoxic stress results from a vicious cycle imposed by the virus in host cells as it hijacks most

intracellular protein machineries [11, 45]. Likewise, cellular senescence was identified in infected alveolar cells/alveospheres of an established primary lung alveolar three-dimensional model, confirming the *in vivo* observations and the findings in Vero cells (**Figure 3B, Figure S5B**).

Senescence-associated secretory phenotype

We found very high expression of both IL-1β and IL-6 by senescent AT2 cells in the lungs of COVID-19 patients, while in the non COVID-19 control cases, including samples from patients with acute pneumonia, expression was very low in the few senescent AT2 cells detected in lung tissue with fibrosis, atelectasia and inflammatory infiltrates ($p<0.0001$) (**Figure 4A-C, Table S1**). As both cytokines are key components of the inflammatory response to SARS-CoV-2, our findings may imply this pattern of inflammation may be due to the SASP as a result of cellular senescence in COVID-19 patients. Likewise, SARS-CoV-2 senescent Vero cells displayed expression of SASP-related cytokines, as assessed by our algorithmic assessment of senescence, supporting our *in vivo* findings (**Figure 3C**).

SARS CoV-2 extra pulmonary dissemination

SARS-CoV-2 immunoreactivity was additionally detected by applying both our 'in house' G2 clone and a commercial one from GeneTek in serial sections of available kidney and liver tissue from one COVID-19 patient (**Figure 5A**). A clear cytoplasmic signal was evident in a number of renal tubules as well as in areas of the liver parenchyma. In contrast, in tissues from non-COVID-19 cases the signal was absent, as expected (**Figure 5A**). Interestingly, by serial section analysis, areas harboring the virus also exhibited senescence (SenTraGor

positivity), implying occurrence of SARS-CoV-2 induced senescence in extra pulmonary sites (**Figure 5B**).

Infected senescent cells and SARS-CoV-2 mutagenesis

We recently hypothesized that senescent cells could represent a source of SARS-CoV-2 quasispecies generation [46]. This assumption was based on the fact that the apoptotic tolerant nature of senescent cells allows the virus to be hosted for longer periods compared to other cells with higher cell turnover [47, 48], thus rendering the SARS-CoV-2 virome more susceptible to host mediated editing. APOBEC enzymes are well known to participate in viral genome editing [12, 33, 49]. Notably, we recently showed these enzymes to be highly expressed in senescent cells [49].

Updating our initial bioinformatic investigation [46], we screened ~ 4,500,000 SARS-CoV-2 strains from the GISAID database [36, 37]. This analysis mostly indicated that the predominant signature of SARS-CoV-2 variants is APOBEC-mediated (**Figure 6**), in line with recent literature [50]. To validate our hypothesis, we proceeded to cell culture infection with two strains isolated from patients and obtained progenies from senescent cells (**Figure 6B**). Next generation sequencing (NGS) analysis demonstrated that the collected viral genomes acquired mutations. Importantly, the predominant pattern was APOBEC-driven, in agreement with the bioinformatic analysis of the GISAID database. Moreover, and in line with our presumption and our previous study [49], the SARS-CoV-2 induced senescent cells demonstrated significantly higher mRNA and protein levels of the APOBEC enzymes, particularly G and H (RNA editing cytoplasmic variants), which are reported to play a pivotal role in viral RNA editing [12, 33, 49]. Other mutation signatures were also

found both in the cell culture isolated virome genomes and in the strains from GISAID, and maybe the outcome of the oxidative stress present in the senescent cells [51].

Discussion

We have demonstrated the presence of SARS-CoV-2 in AT2 cells of patients who died from COVID-19 using our novel and a commercial anti-SARS-CoV-2 antibody against its spike protein and by electron microscopy. We have shown for the first time following the senescence detecting algorithm *in vivo* that a proportion of SARS-CoV-2-infected AT2 cells exhibit features of cellular senescence (as demonstrated by significantly increased staining with the novel senescence marker SenTraGor^{TM} and also of p16^{INK4A}) [12, 27, 35]. In this respect, our investigation encompassing serial section analysis and co-staining is the first to demonstrate *in vivo* which cells are truly senescent and infected. The finding that in age-matched non-COVID-19 controls, including lung tissue samples from a cohort of patients with acute pneumonia, the percentage of senescent cells was much lower (1-2%) than that of the COVID-19 patients (8-21%), strongly indicates that SARS-CoV-2 triggers senescence. To confirm that SARS-CoV-2 induces cellular senescence *per se*, we demonstrated that infection of epithelial cells with SARS-CoV-2 virus (B.1.222 strain) *in vitro* increased SenTraGor^{TM} staining and induced DNA damage, measured by increased γ-H2AX expression. Importantly, we found that inhibition of ATM (ataxia-telangiectasia-mutated protein kinase), an apical orchestrator of the DNA damage response pathway, dramatically reduced senescence in infected samples, suggesting SARS-CoV-2 induced senescence being mediated by DNA damage and activation of the DNA damage response pathway. In line with our *in vivo* and *in vitro* findings, SARS-CoV-2 induced senescence was identified in a previously established

primary lung alveolar three-dimensional model [32]. The fact that alveospheres underwent gentle mechanical manipulations is unlikely to have contributed to the occurrence of senescence, given that such interventions are frequently applied on 3D organoid systems and no senescence phenotypes have been reported nor are evident from the post-infection proliferation rates and culture [52].

We also demonstrated that cells infected with SARS-CoV-2 exhibit high expression of IL-1β and IL-6, both components of the SASP and implicated in systemic features of severe COVID-19 [3, 4]. Therefore, our *in vitro* and *in vivo* findings suggest that SARS-CoV-2 attaches to AT2 cells via ACE2 to infect these cells and through activation of DNA damage response signalling roots, induces cellular senescence and associated proinflammatory phenotype (SASP). In line with our observations, Lee et al recently demonstrated that SARS-CoV-2-induced senescence exhibited enhanced γ-H2AX DNA damage foci that were abrogated by the reactive oxygen species (ROS) scavenger N-acetylcysteine (NAC) [29], suggesting implication of ROS and oxidative stress (Figure **S8**). Moreover, infected cells displayed SASP-positive senescence mediated by p53 and activation of cGAS/STING signaling pathway [29]. They also demonstrated that senolytics reduced COVID-19 lung disease and inflammation in infected hamsters and mice [29], further suggesting SASP as an outcome of viral induced senescence. Camell et al also reported that treatment with senolytics of old mice infected with a SARS-CoV-2–related mouse β-coronavirus reduced inflammation [53]. Based on our findings and recent evidence a potential mechanistic scenario could be the following **(Figure S8)**: upon entrance, the virus highjacks certain energy consuming functions related to RNA processing, translation and the ER [11]. Thus, an energy shift occurs resulting in increased ROS production, oxidative stress and DNA damage/DNA Damage Response (DDR) pathway activation. In addition, DDR and the subsequent cell cycle arrest may be driven by an

interaction of Coronavirus nsp13 protein and DNA polymerase δ [54] and SASP via the cGAS/STING and other DNA damage dependent pathways **(Figure S8)**. Therefore, our previous work showing that DNA damage/DDR is a potent inducer of senescence, signifies its importance in the establishment of the viral induced senescence phenotype [31].

Senescent cells are in a state of cell cycle arrest but remain metabolically active and secrete a typical profile of inflammatory proteins known as the SASP. SASP components include the proinflammatory cytokines IL-1β and IL-6, which are elevated in plasma of COVID-19 patients that have acute respiratory distress syndrome (ARDS) or systemic inflammatory features. We demonstrate that in COVID-19, senescence alters the properties and function of AT2 cells, producing cytokines that could be released into the systemic circulation, amplifying and perpetuating chronic inflammation. Of course, the availability of tissue samples and the absence of more refined COVID-19 *in vitro* and *in vivo* models make it difficult to draw robust conclusions. It is likely that SARS-CoV-2 spreads from epithelial cells in the lower airways to infect AT2 cells in the alveolar walls, which express ACE2, and causes local senescence and inflammation via SASP in the lung. In line with this notion, it has been previously reported *in vitro* that cellular senescence has also a role as a natural antiviral defence mechanism and that SASP acts as the major contributor of this response, activating and recruiting the immune system to clear out the infection [21, 22]. Subsequently, other cellular compartments (stem/progenitor, endothelial and inflammatory cells) may be affected via different cell and non-cell autonomous mechanisms, leading to aberrant immune responses, chronic inflammation, tissue dysfunction and/or fibrosis and eventually to lung damage and failure [26, 55]. In particular, senescence in stem/progenitor cells impairs lung regenerative capacity. Immunosenescence results in elevated neutrophils-to-lymphocytes ratio (NLR) and high IL-6 production. In addition, IL-1, IL-6, CXCL8 and TNF-α

might be crucial for maintaining chronic inflammation and TGF-β, PAI-1, and MMPs might favour fibrosis via the expression of fibrotic genes (ACTA2, COL1A1, COL1A2, and FN1) in the surrounding microenvironment. The virus may then enter the circulation and senescence may subsequently spread systemically to affect other organs (**Figure 5**), leading to multi-organ failure/multi-morbidity and death in the acute phase [1, 25], or leading to post-acute sequelae of COVID-19 (PASC or long-COVID), an evolving syndrome with long-term complications [26, 56]. In this manner, senescence could also predispose to disease severity upon re-infection by SARS-CoV-2 or infection by other viruses and even negatively impact vaccine efficacy, similarly to what has been proposed for aged individuals [26].

An additional implication relates to the prolonged survival of senescent cells that are infected with the virus, as senescent cells are resistant to apoptosis and clearance by efferocytosis [12, 14]. Such a context can provide an extended time "window" for virus replication, therefore exposing its genome to host-mediated editing. Along this vein we showed that the senescent cell compartment acts as a "fertile" environment for mutational evolution of the virus, as it is more susceptible to APOBEC-3G and 3H RNA editing (**Figure 6)** [33, 49]. Of course, other mechanisms extending survival and replication of SARS-CoV-2 may take place. Coronaviruses code for an important multifunctional enzyme termed papain-like protease (PLP) that exerts intrinsic deubiquitinating and deISGylating activities. The latter is related to interferon-stimulated genes (ISG) up-regulation and can serve to antagonize the host's immune response that would otherwise hinder infection [57]. In this manner increased and prolonged viral replication and exposure of its genome to host mediated editing and quasispecies generation could also occur. Taking into account that interferons are known senescence inducers, the picture gets even more complicated, rendering difficult to discriminate IGS-mediated mechanisms from that involving virally-induced senescence

[58]. Of course, additional studies are needed and the guideline algorithmic approach for *in vivo* senescence assessment, followed in the current work, is anticipated to clarify in the future a lot of unanswered questions in clinical settings [12, 27]. Notably, in the recently identified Omicron (B.1.1.529) SARS-CoV-2 variant/strain the APOBEC signature was identified as the predominant mutational profile (**Figure S9**). To better understand the role of APOBEC in the generation of viral mutations, inhibition of APOBEC proteins by RNA interference would be valuable. However, this is very challenging, since APOBEC suppression induces DNA damage and sensitises cells to stress induced death [59-61]. Interestingly and in line with our concept linking cellular senescence with viral mutagenesis, by conducting a bioinformatic analysis, we found that viruses bypassing cellular senescence (oncogenic) exhibit a significant lower mutation burden compared to viruses inducing senescence (**Figure S10**). Given that mutations can affect the effectiveness of vaccines, our findings could imply a potential implication of viral induced senescence in vaccination strategies. Further studies are required towards this root.

Despite the fact that up to the present this is the largest clinical study demonstrating virally-induced senescence by SARS-CoV-2, a limitation of our study is the relatively small sample size of the COVID-19 lung autopsies, due to difficulty of accessing this rare material, given that the autopsies are limited and were performed only in the initial phase of the COVID-19 outbreak in order to identify the pathological basis of this new entity. Another limitation due to the nature of the disease is that pathological features, such as cellular senescence in lungs, can only be investigated in cadaverous material, which represents the most severe outcome of the spectrum of COVID-19 clinical manifestations. Therefore, evaluation of senescence in less severe conditions is not currently feasible. Moreover, in our study we examined 18 cases of aspiration pneumonia, which displayed similar degrees of

senescence to other non-infected control cases. It would be interesting to extend these studies in other types of pneumonia. However, material from patients with an acute but not COVID-19 related inflammatory response is rare, given that these patients commonly recover following treatment and in the infrequent cases of fatal outcome autopsy is rarely performed.

Overall, SARS-CoV-2 induced senescence justifies the therapeutic application of senotherapeutics for the treatment of COVID-19 patients and possibly for long-COVID syndromes [56]. In line, quercetin was recently tested against standard care in two randomized clinical trials (ClinicalTrials.gov identifiers NCT04578158 and NCT04861298) in patients with confirmed SARS-CoV-2 infection and mild COVID-19-associated symptoms. In both trials, senolytic intervention led to clinical improvement [62, 63]. Overall, these data imply the beneficial role of senolytics in significantly improving the outcome during SARS-CoV-2 infection.

Acknowledgements:

We would like to thank Konstantinos Ntostoglou for his valuable help in preparing the material. We acknowledge support in RNA sequencing by the Greek Research Infrastructure for Personalised Medicine (pMED-GR) (MIS 5002802), which is implemented under the Action “Reinforcement of the Research and Innovation Infrastructure”, funded by the Operational Programme "Competitiveness, Entrepreneurship and Innovation" (NSRF 2014-2020) and co-financed by Greece and the European Union (European Regional Development Fund). This work was supported by the: National Public Investment Program of the Ministry of Development and Investment / General Secretariat for Research and Technology, in the framework of the Flagship Initiative to address SARS-CoV-2 (2020ΣΕ01300001); Horizon 2020

Marie Sklodowska-Curie training program no. 722729 (SYNTRAIN); Welfare Foundation for Social & Cultural Sciences, Athens, Greece (KIKPE); H. Pappas donation; Hellenic Foundation for Research and Innovation (HFRI) grants no. 775 and 3782 and NKUA-SARG grant 70/3/8916. KP is financially supported by National Heart & Lung Institute – Imperial College London and a British Heart Foundation Project Grant (PG/19/75/34686).

Disclosure/Conflict of Interest

PB receives research funding from AstraZeneca and Boehringer-Ingelheim and is a scientific advisor to AstraZeneca, Boehringer-Ingelheim, Epi-Endo, Novartis, Pieris and Teva. The other authors wish to declare no conflict of interest.

Figure Legends

Figure 1: Detection of SARS-CoV-2 in lung cells from patients who died of COVID-19. A. Representative images of SARS-CoV-2 (G2 mab) immunohistochemistry (IHC) staining in COVID-19 autopsy lung tissue. Competition with anti-peptide (S protein) showing specificity of the G2 immunostaining. Verification of G2 immunopositivity with a commercial anti-S antibody (clone 1A9 clone, Genetek). Representative negative control immunostaining in non-COVID-19 lung tissues. Graph shows quantification of SARS-CoV-2 staining in the lung samples. **B.** Detection of SARS-CoV-2 in AT2 cells (confirmed by positive TTF-1 and Surfactant Protein B (SP-B) staining) and in ACE2-expressing cells. Double immunostaining is shown for SARS-CoV-2 and TTF-1. **C.** Detection of SARS-CoV-2 by transmission electron microscopy (EM) in a representative COVID-19 patient. Presence of SARS-CoV-2 within AT2 cells (**i, ii**) and of virions in the proximity of the endoplasmic reticulum (**iii, iv**) as well as in cytoplasmic vesicles (**iii, v-vi**). Corresponding scale bars are depicted. AT2: alveolar type 2 cells; ACE2: Angiotensin-Converting Enzyme 2; ****Statistical significance: $p < 0.0001$.

Figure 2: Senescence in SARS-CoV-2 infected cells. A. Representative images of SARS-CoV-2, SenTraGor^{TM} (senescence) and ACE-2 staining in serial sections of COVID-19 lung tissue (**1**)**.** Double-immunostaining analysis for SARS-CoV-2, SenTraGor^{TM} (senescence), p16^{INK4A}, TTF-1 and Surfactant Protein B (SP-B) in COVID-19 lung tissue (**2**)**. B.** Representative results from serial staining for SARS-CoV-2, SenTraGor^{TM} (senescence) and ACE-2, and double-staining for SARS-CoV-2 and p16^{INK4A} in non-COVID-19 lung tissue**. C.** Graphs showing increased expression of SenTraGor^{TM} and p16^{INK4A} in COVID-19 lung tissue**.** Corresponding scale bars are depicted. ****Statistical significance: $p < 0.0001$.

Figure 3. SARS-CoV-2 induced senescence in Vero cells and alveospheres. A. SARS-CoV-2 presence (**1**), senescence induction (**2**), cellular proliferation (**3**) and DNA damage activation (**4**), with corresponding quantitative histograms, in Vero cells with and without SARS-CoV-2 infection (17 days post infection). **B.** Senescence induction (assessed by SenTraGor and $p21^{WAF1/CIP1}$ staining) in alveolar cells (alveospheres) of a primary lung alveolar three-dimensional model following SARS-CoV-2 infection (black arrows) in comparison to non senescent ones (yellow arrows). Absence of senescence is clearly evident in non infected alveolar cells. **C.** Graph showing induction of SASP related cytokines following SARS-CoV-2 infection of Vero cells (mRNA expression – normalized against β2-microglobulin mRNA expression) **Statistical significance: $p < 0.01$.

Figure 4: Senescence associated secretory phenotype (SASP) in COVID-19 lung tissues. A. Representative staining results (at low and high magnification) of SenTraGor™, IL-6, IL-1β and TTF-1 and/or Surfactant Protein B (SP-B) in corresponding serial sections (**1**) and as double immunostaining analysis (**2**) of COVID-19 lung tissue. Original magnification: 400x**. B.** Representative staining results showing absence or minimal levels of SenTraGor™, IL-6 and IL-1β in age-matched non-COVID-19 control samples. Corresponding scale bars are depicted. IL-1 β: Interleukin 1β; IL-6: Interleukin-6; **** Statistical significance: $p < 0.001$.

Figure 5: SARS-CoV-2 dissemination in extra pulmonary sites. A. Representative staining results of SARS-CoV-2 in the kidney and the liver of a COVID-19 patient. Absence of the immunohistochemical signal is evident in the corresponding tissues of a representative non COVID-19 case. **B.** Serial section analysis the representative COVID-19 case (see panel A)

depicting concurrent positivity for SARS-CoV-2 and the senescence marker (SenTraGor^{TM}) in cells of the liver and kidney.

Figure 6: Infected senescent cells as a putative source for SARS-CoV-2 quasi-species variant generation. A. Schematic layout presenting the identification of APOBEC-mediated mutations in the genome of 4,672,296 SARS-CoV-2 strains available in GISAID database. For algorithmic assessment see **Figure S7** and corresponding section in Materials & Methods. **B.** Identification of SARS-CoV-2 mutations acquired in senescent cells in two strains (i: B.1.222 and ii: B.1) isolated from two different patients, following cell culture infection for the depicted time periods. Yellow bars show the frequency of C→U substitutions observed in the GISAID database in the NGS read counts (green pileups) and red bars depict the C→U frequency of mutation observed, post infection of cells in the current study, in the genome of the two employed SARS-CoV-2 strains. These sites are ranked as highest relatively to the C→U counts as observed from the GISAID database. The genomic sequences flanking each C→U are also presented, while their co-ordinates are shown relative to the superimposed SARS-CoV-2 genome. NGS (Next Generation Sequencing) reads were confirmed in triplicate reads.

Table 1

Table 1: Summary of clinical characteristics of patients

Participants	COVID-19	Controls	Non-COVID pneumonia
Number (n)	11	25	18
Sex (M/F)	8/3	17/8	10/8
Age (years)	71±5	70±2	75±1
Smokers (current or ex-)	3	25	18
Acute pneumonia	11	0	18
Comorbidities			
COPD	4	14	0
Cardiovascular disease	7	9	18
Diabetes	4	2	8
Chronic kidney disease	2	0	1
Malignancy	2 (lymphoma, brain tumor)	25 (lung cancer)	0

Values are expressed as means ± SEM. COPD indicates chronic obstructive pulmonary disease; M = male; F = female. Cardiovascular disease: includes ischemic heart disease, hypertension, cardiomyopathy, pulmonary embolism, peripheral artery disease and stroke. All non-COVID samples were obtained from distal lung tissue to resected lung carcinoma (lobectomy or pneumonectomy). All non-COVID acute pneumonia samples were from patients with aspiration pneumonia.

References

1. Hu B, Guo H, Zhou P, Shi ZL. Characteristics of SARS-CoV-2 and COVID-19. *Nature reviews Microbiology* 2021: 19(3): 141-154.
2. Robba C, Battaglini D, Ball L, Patroniti N, Loconte M, Brunetti I, Vena A, Giacobbe DR, Bassetti M, Rocco PRM, Pelosi P. Distinct phenotypes require distinct respiratory management strategies in severe COVID-19. *Respiratory physiology & neurobiology* 2020: 279: 103455.
3. Del Valle DM, Kim-Schulze S, Huang HH, Beckmann ND, Nirenberg S, Wang B, Lavin Y, Swartz TH, Madduri D, Stock A, Marron TU, Xie H, Patel M, Tuballes K, Van Oekelen O, Rahman A, Kovatch P, Aberg JA, Schadt E, Jagannath S, Mazumdar M, Charney AW, Firpo-Betancourt A, Mendu DR, Jhang J, Reich D, Sigel K, Cordon-Cardo C, Feldmann M, Parekh S, Merad M, Gnjatic S. An inflammatory cytokine signature predicts COVID-19 severity and survival. *Nature medicine* 2020: 26(10): 1636-1643.
4. Tang Y, Liu J, Zhang D, Xu Z, Ji J, Wen C. Cytokine Storm in COVID-19: The Current Evidence and Treatment Strategies. *Frontiers in immunology* 2020: 11: 1708.
5. Poland GA, Ovsyannikova IG, Kennedy RB. SARS-CoV-2 immunity: review and applications to phase 3 vaccine candidates. *Lancet (London, England)* 2020: 396(10262): 1595-1606.
6. Zhang F, Gan R, Zhen Z, Hu X, Li X, Zhou F, Liu Y, Chen C, Xie S, Zhang B, Wu X, Huang Z. Adaptive immune responses to SARS-CoV-2 infection in severe versus mild individuals. *Signal transduction and targeted therapy* 2020: 5(1): 156.
7. Rouse BT, Sehrawat S. Immunity and immunopathology to viruses: what decides the outcome? *Nature reviews Immunology* 2010: 10(7): 514-526.
8. Mocarski ES, Upton JW, Kaiser WJ. Viral infection and the evolution of caspase 8-regulated apoptotic and necrotic death pathways. *Nature reviews Immunology* 2011: 12(2): 79-88.
9. Braciale TJ, Sun J, Kim TS. Regulating the adaptive immune response to respiratory virus infection. *Nature reviews Immunology* 2012: 12(4): 295-305.
10. Fan Y, Sanyal S, Bruzzone R. Breaking Bad: How Viruses Subvert the Cell Cycle. *Frontiers in cellular and infection microbiology* 2018: 8: 396.
11. Hekman RM, Hume AJ, Goel RK, Abo KM, Huang J, Blum BC, Werder RB, Suder EL, Paul I, Phanse S, Youssef A, Alysandratos KD, Padhorny D, Ojha S, Mora-Martin A, Kretov D, Ash PEA, Verma M, Zhao J, Patten JJ, Villacorta-Martin C, Bolzan D, Perea-Resa C, Bullitt E, Hinds A, Tilston-Lunel A, Varelas X, Farhangmehr S, Braunschweig U, Kwan JH, McComb M, Basu A, Saeed M, Perissi V, Burks EJ, Layne MD, Connor JH, Davey R, Cheng JX, Wolozin BL, Blencowe BJ, Wuchty S, Lyons SM, Kozakov D, Cifuentes D, Blower M, Kotton DN, Wilson AA, Mühlberger E, Emili A. Actionable Cytopathogenic Host Responses of Human Alveolar Type 2 Cells to SARS-CoV-2. *Molecular cell* 2021: 81(1): 212.
12. Gorgoulis V, Adams PD, Alimonti A, Bennett DC, Bischof O, Bishop C, Campisi J, Collado M, Evangelou K, Ferbeyre G, Gil J, Hara E, Krizhanovsky V, Jurk D, Maier AB, Narita M, Niedernhofer L, Passos JF, Robbins PD, Schmitt CA, Sedivy J, Vougas K, von Zglinicki T, Zhou D, Serrano M, Demaria M. Cellular Senescence: Defining a Path Forward. *Cell* 2019: 179(4): 813-827.
13. Rendeiro AF, Ravichandran H, Bram Y, Salvatore S, Borczuk A, Elemento O, Schwartz RE. The spatio-temporal landscape of lung pathology in SARS-CoV-2 infection. *medRxiv : the preprint server for health sciences* 2020.
14. Childs BG, Baker DJ, Kirkland JL, Campisi J, van Deursen JM. Senescence and apoptosis: dueling or complementary cell fates? *EMBO reports* 2014: 15(11): 1139-1153.
15. Myrianthopoulos V, Evangelou K, Vasileiou PVS, Cooks T, Vassilakopoulos TP, Pangalis GA, Kouloukoussa M, Kittas C, Georgakilas AG, Gorgoulis VG. Senescence and senotherapeutics: a new field in cancer therapy. *Pharmacology & therapeutics* 2019: 193: 31-49.
16. Özcan S, Alessio N, Acar MB, Mert E, Omerli F, Peluso G, Galderisi U. Unbiased analysis of senescence associated secretory phenotype (SASP) to identify common components following different genotoxic stresses. *Aging* 2016: 8(7): 1316-1329.

17. Basisty N, Kale A, Jeon OH, Kuehnemann C, Payne T, Rao C, Holtz A, Shah S, Sharma V, Ferrucci L, Campisi J, Schilling B. A proteomic atlas of senescence-associated secretomes for aging biomarker development. *PLoS biology* 2020: 18(1): e3000599.
18. Faget DV, Ren Q, Stewart SA. Unmasking senescence: context-dependent effects of SASP in cancer. *Nature reviews Cancer* 2019: 19(8): 439-453.
19. Barnes PJ, Baker J, Donnelly LE. Cellular Senescence as a Mechanism and Target in Chronic Lung Diseases. *American journal of respiratory and critical care medicine* 2019: 200(5): 556-564.
20. Schneider JL, Rowe JH, Garcia-de-Alba C, Kim CF, Sharpe AH, Haigis MC. The aging lung: Physiology, disease, and immunity. *Cell* 2021: 184(8): 1990-2019.
21. Baz-Martínez M, Da Silva-Álvarez S, Rodríguez E, Guerra J, El Motiam A, Vidal A, García-Caballero T, González-Barcia M, Sánchez L, Muñoz-Fontela C, Collado M, Rivas C. Cell senescence is an antiviral defense mechanism. *Scientific reports* 2016: 6: 37007.
22. Seoane R, Vidal S, Bouzaher YH, El Motiam A, Rivas C. The Interaction of Viruses with the Cellular Senescence Response. *Biology* 2020: 9(12).
23. Chuprin A, Gal H, Biron-Shental T, Biran A, Amiel A, Rozenblatt S, Krizhanovsky V. Cell fusion induced by ERVWE1 or measles virus causes cellular senescence. *Genes & development* 2013: 27(21): 2356-2366.
24. Kelley WJ, Zemans RL, Goldstein DR. Cellular senescence: friend or foe to respiratory viral infections? *The European respiratory journal* 2020: 56(6).
25. Kohli J, Veenstra I, Demaria M. The struggle of a good friend getting old: cellular senescence in viral responses and therapy. *EMBO reports* 2021: 22(4): e52243.
26. Nehme J, Borghesan M, Mackedenski S, Bird TG, Demaria M. Cellular senescence as a potential mediator of COVID-19 severity in the elderly. *Aging cell* 2020: 19(10): e13237.
27. Kohli J, Wang B, Brandenburg SM, Basisty N, Evangelou K, Varela-Eirin M, Campisi J, Schilling B, Gorgoulis V, Demaria M. Algorithmic assessment of cellular senescence in experimental and clinical specimens. *Nature protocols* 2021: 16(5): 2471-2498.
28. Evangelou K, Veroutis D, Foukas PG, Paschalaki K, Lagopati N, Dimitriou M, Papaspyropoulos A, Hazapis O, Polyzou A, Havaki S, Kotsinas A, Kittas C, Tzioufas AG, de Leval L, Vassilakos D, Tsiodras S, Karakasiliotis I, Barnes PJ, Gorgoulis VG. SARS-CoV-2 infects lung epithelial cells and induces senescence and an inflammatory response in patients with severe COVID-19. *bioRxiv* 2021: 2021.2001.2002.424917.
29. Lee S, Yu Y, Trimpert J, Benthani F, Mairhofer M, Richter-Pechanska P, Wyler E, Belenki D, Kaltenbrunner S, Pammer M, Kausche L, Firsching TC, Dietert K, Schotsaert M, Martínez-Romero C, Singh G, Kunz S, Niemeyer D, Ghanem R, Salzer HJF, Paar C, Mülleder M, Uccellini M, Michaelis EG, Khan A, Lau A, Schönlein M, Habringer A, Tomasits J, Adler JM, Kimeswenger S, Gruber AD, Hoetzenecker W, Steinkellner H, Purfürst B, Motz R, Di Pierro F, Lamprecht B, Osterrieder N, Landthaler M, Drosten C, García-Sastre A, Langer R, Ralser M, Eils R, Reimann M, Fan DNY, Schmitt CA. Virus-induced senescence is a driver and therapeutic target in COVID-19. *Nature* 2021.
30. Gorgoulis VG, Vassiliou LV, Karakaidos P, Zacharatos P, Kotsinas A, Liloglou T, Venere M, Ditullio RA, Jr., Kastrinakis NG, Levy B, Kletsas D, Yoneta A, Herlyn M, Kittas C, Halazonetis TD. Activation of the DNA damage checkpoint and genomic instability in human precancerous lesions. *Nature* 2005: 434(7035): 907-913.
31. Bartkova J, Rezaei N, Liontos M, Karakaidos P, Kletsas D, Issaeva N, Vassiliou LV, Kolettas E, Niforou K, Zoumpourlis VC, Takaoka M, Nakagawa H, Tort F, Fugger K, Johansson F, Sehested M, Andersen CL, Dyrskjot L, Ørntoft T, Lukas J, Kittas C, Helleday T, Halazonetis TD, Bartek J, Gorgoulis VG. Oncogene-induced senescence is part of the tumorigenesis barrier imposed by DNA damage checkpoints. *Nature* 2006: 444(7119): 633-637.
32. Mulay A, Konda B, Garcia G, Jr., Yao C, Beil S, Villalba JM, Koziol C, Sen C, Purkayastha A, Kolls JK, Pociask DA, Pessina P, de Aja JS, Garcia-de-Alba C, Kim CF, Gomperts B, Arumugaswami V, Stripp BR. SARS-CoV-2 infection of primary human lung epithelium for COVID-19 modeling and drug discovery. *Cell reports* 2021: 35(5): 109055.

33. Komseli ES, Pateras IS, Krejsgaard T, Stawiski K, Rizou SV, Polyzos A, Roumelioti FM, Chiourea M, Mourkioti I, Paparouna E, Zampetidis CP, Gumeni S, Trougakos IP, Pefani DE, O'Neill E, Gagos S, Eliopoulos AG, Fendler W, Chowdhury D, Bartek J, Gorgoulis VG. A prototypical non-malignant epithelial model to study genome dynamics and concurrently monitor micro-RNAs and proteins in situ during oncogene-induced senescence. *BMC genomics* 2018: 19(1): 37.
34. Lagopati N, Tsioli P, Mourkioti I, Polyzou A, Papaspyropoulos A, Zafiropoulos A, Evangelou K, Sourvinos G, Gorgoulis VG. Sample pooling strategies for SARS-CoV-2 detection. *Journal of virological methods* 2021: 289: 114044.
35. Evangelou K, Lougiakis N, Rizou SV, Kotsinas A, Kletsas D, Muñoz-Espín D, Kastrinakis NG, Pouli N, Marakos P, Townsend P, Serrano M, Bartek J, Gorgoulis VG. Robust, universal biomarker assay to detect senescent cells in biological specimens. *Aging cell* 2017: 16(1): 192-197.
36. Elbe S, Buckland-Merrett G. Data, disease and diplomacy: GISAID's innovative contribution to global health. *Glob Chall* 2017: 1(1): 33-46.
37. Shu Y, McCauley J. GISAID: Global initiative on sharing all influenza data - from vision to reality. *Euro Surveill* 2017: 22(13).
38. Belogiannis K, Florou VA, Fragkou PC, Ferous S, Chatzis L, Polyzou A, Lagopati N, Vassilakos D, Kittas C, Tzioufas AG, Tsiodras S, Sourvinos G, Gorgoulis VG. SARS-CoV-2 Antigenemia as a Confounding Factor in Immunodiagnostic Assays: A Case Study. *Viruses* 2021: 13(6).
39. Wang Q, Zhang Y, Wu L, Niu S, Song C, Zhang Z, Lu G, Qiao C, Hu Y, Yuen KY, Wang Q, Zhou H, Yan J, Qi J. Structural and Functional Basis of SARS-CoV-2 Entry by Using Human ACE2. *Cell* 2020: 181(4): 894-904.e899.
40. Wurtz N, Penant G, Jardot P, Duclos N, La Scola B. Culture of SARS-CoV-2 in a panel of laboratory cell lines, permissivity, and differences in growth profile. *Eur J Clin Microbiol Infect Dis* 2021: 40(3): 477-484.
41. Chu H, Chan JF, Yuen TT, Shuai H, Yuan S, Wang Y, Hu B, Yip CC, Tsang JO, Huang X, Chai Y, Yang D, Hou Y, Chik KK, Zhang X, Fung AY, Tsoi HW, Cai JP, Chan WM, Ip JD, Chu AW, Zhou J, Lung DC, Kok KH, To KK, Tsang OT, Chan KH, Yuen KY. Comparative tropism, replication kinetics, and cell damage profiling of SARS-CoV-2 and SARS-CoV with implications for clinical manifestations, transmissibility, and laboratory studies of COVID-19: an observational study. *Lancet Microbe* 2020: 1(1): e14-e23.
42. Matsuyama S, Ujike M, Morikawa S, Tashiro M, Taguchi F. Protease-mediated enhancement of severe acute respiratory syndrome coronavirus infection. *Proceedings of the National Academy of Sciences of the United States of America* 2005: 102(35): 12543-12547.
43. Osada N, Kohara A, Yamaji T, Hirayama N, Kasai F, Sekizuka T, Kuroda M, Hanada K. The genome landscape of the african green monkey kidney-derived vero cell line. *DNA research : an international journal for rapid publication of reports on genes and genomes* 2014: 21(6): 673-683.
44. Zhao J, Zhang L, Lu A, Han Y, Colangelo D, Bukata C, Scibetta A, Yousefzadeh MJ, Li X, Gurkar AU, McGowan SJ, Angelini L, O'Kelly R, Li H, Corbo L, Sano T, Nick H, Pola E, Pilla SPS, Ladiges WC, Vo N, Huard J, Niedernhofer LJ, Robbins PD. ATM is a key driver of NF-κB-dependent DNA-damage-induced senescence, stem cell dysfunction and aging. *Aging* 2020: 12(6): 4688-4710.
45. Gorgoulis VG, Pefani DE, Pateras IS, Trougakos IP. Integrating the DNA damage and protein stress responses during cancer development and treatment. *The Journal of pathology* 2018: 246(1): 12-40.
46. Karakasiliotis I, Lagopati N, Evangelou K, Gorgoulis VG. Cellular senescence as a source of SARS-CoV-2 quasispecies. *The FEBS journal* 2021.
47. Zamaraev AV, Zhivotovsky B, Kopeina GS. Viral Infections: Negative Regulators of Apoptosis and Oncogenic Factors. *Biochemistry (Mosc)* 2020: 85(10): 1191-1201.
48. Li S, Zhang Y, Guan Z, Li H, Ye M, Chen X, Shen J, Zhou Y, Shi ZL, Zhou P, Peng K. SARS-CoV-2 triggers inflammatory responses and cell death through caspase-8 activation. *Signal transduction and targeted therapy* 2020: 5(1): 235.

49. Venkatesan S, Angelova M, Puttick C, Zhai H, Caswell DR, Lu WT, Dietzen M, Galanos P, Evangelou K, Bellelli R, Lim EL, Watkins TBK, Rowan A, Teixeira VH, Zhao Y, Chen H, Ngo B, Zalmas LP, Al Bakir M, Hobor S, Grönroos E, Pennycuick A, Nigro E, Campbell BB, Brown WL, Akarca AU, Marafioti T, Wu MY, Howell M, Boulton SJ, Bertoli C, Fenton TR, de Bruin RAM, Maya-Mendoza A, Santoni-Rugiu E, Hynds RE, Gorgoulis VG, Jamal-Hanjani M, McGranahan N, Harris RS, Janes SM, Bartkova J, Bakhoum SF, Bartek J, Kanu N, Swanton C. Induction of APOBEC3 Exacerbates DNA Replication Stress and Chromosomal Instability in Early Breast and Lung Cancer Evolution. *Cancer discovery* 2021: 11(10): 2456-2473.
50. Ratcliff J, Simmonds P. Potential APOBEC-mediated RNA editing of the genomes of SARS-CoV-2 and other coronaviruses and its impact on their longer term evolution. *Virology* 2021: 556: 62-72.
51. Li Z, Chen X, Liu Z, Ye W, Li L, Qian L, Ding H, Li P, Aung LHH. Recent Advances: Molecular Mechanism of RNA Oxidation and Its Role in Various Diseases. *Front Mol Biosci* 2020: 7: 184.
52. Heo I, Dutta D, Schaefer DA, Iakobachvili N, Artegiani B, Sachs N, Boonekamp KE, Bowden G, Hendrickx APA, Willems RJL, Peters PJ, Riggs MW, O'Connor R, Clevers H. Modelling Cryptosporidium infection in human small intestinal and lung organoids. *Nat Microbiol* 2018: 3(7): 814-823.
53. Camell CD, Yousefzadeh MJ, Zhu Y, Prata L, Huggins MA, Pierson M, Zhang L, O'Kelly RD, Pirtskhalava T, Xun P, Ejima K, Xue A, Tripathi U, Espindola-Netto JM, Giorgadze N, Atkinson EJ, Inman CL, Johnson KO, Cholensky SH, Carlson TW, LeBrasseur NK, Khosla S, O'Sullivan MG, Allison DB, Jameson SC, Meves A, Li M, Prakash YS, Chiarella SE, Hamilton SE, Tchkonia T, Niedernhofer LJ, Kirkland JL, Robbins PD. Senolytics reduce coronavirus-related mortality in old mice. *Science (New York, NY)* 2021: 373(6552).
54. Victor J, Deutsch J, Whitaker A, Lamkin EN, March A, Zhou P, Botten JW, Chatterjee N. SARS-CoV-2 triggers DNA damage response in Vero E6 cells. *Biochem Biophys Res Commun* 2021: 579: 141-145.
55. Meyer K, Patra T, Vijayamahantesh, Ray R. SARS-CoV-2 Spike Protein Induces Paracrine Senescence and Leukocyte Adhesion in Endothelial Cells. *J Virol* 2021: 95(17): e0079421.
56. Nalbandian A, Sehgal K, Gupta A, Madhavan MV, McGroder C, Stevens JS, Cook JR, Nordvig AS, Shalev D, Sehrawat TS, Ahluwalia N, Bikdeli B, Dietz D, Der-Nigoghossian C, Liyanage-Don N, Rosner GF, Bernstein EJ, Mohan S, Beckley AA, Seres DS, Choueiri TK, Uriel N, Ausiello JC, Accili D, Freedberg DE, Baldwin M, Schwartz A, Brodie D, Garcia CK, Elkind MSV, Connors JM, Bilezikian JP, Landry DW, Wan EY. Post-acute COVID-19 syndrome. *Nature medicine* 2021: 27(4): 601-615.
57. Clemente V, D'Arcy P, Bazzaro M. Deubiquitinating Enzymes in Coronaviruses and Possible Therapeutic Opportunities for COVID-19. *Int J Mol Sci* 2020: 21(10).
58. Frisch SM, MacFawn IP. Type I interferons and related pathways in cell senescence. *Aging cell* 2020: 19(10): e13234.
59. Wang Y, Wu S, Zheng S, Wang S, Wali A, Ezhilarasan R, Sulman EP, Koul D, Alfred Yung WK. APOBEC3G acts as a therapeutic target in mesenchymal gliomas by sensitizing cells to radiation-induced cell death. *Oncotarget* 2017: 8(33): 54285-54296.
60. Botvinnik A, Shivam P, Smith Y, Sharma G, Olshevsky U, Moshel O, Manevitch Z, Climent N, Oliva H, Britan-Rosich E, Kotler M. APOBEC3G rescues cells from the deleterious effects of DNA damage. *The FEBS journal* 2021: 288(20): 6063-6077.
61. Prabhu P, Shandilya SM, Britan-Rosich E, Nagler A, Schiffer CA, Kotler M. Inhibition of APOBEC3G activity impedes double-stranded DNA repair. *The FEBS journal* 2016: 283(1): 112-129.
62. Di Pierro F, Iqtadar S, Khan A, Ullah Mumtaz S, Masud Chaudhry M, Bertuccioli A, Derosa G, Maffioli P, Togni S, Riva A, Allegrini P, Khan S. Potential Clinical Benefits of Quercetin in the Early Stage of COVID-19: Results of a Second, Pilot, Randomized, Controlled and Open-Label Clinical Trial. *Int J Gen Med* 2021: 14: 2807-2816.
63. Di Pierro F, Derosa G, Maffioli P, Bertuccioli A, Togni S, Riva A, Allegrini P, Khan A, Khan S, Khan BA, Altaf N, Zahid M, Ujjan ID, Nigar R, Khushk MI, Phulpoto M, Lail A, Devrajani BR, Ahmed S. Possible Therapeutic Effects of Adjuvant Quercetin Supplementation Against Early-Stage COVID-19 Infection: A Prospective, Randomized, Controlled, and Open-Label Study. *Int J Gen Med* 2021: 14: 2359-2366.

FIGURE 1

A.

COVID-19 Lung

Anti-SARS-CoV-2 ab

Anti-SARS-CoV-2 ab/ S protein (1:10)

Patient #1

Patient #2

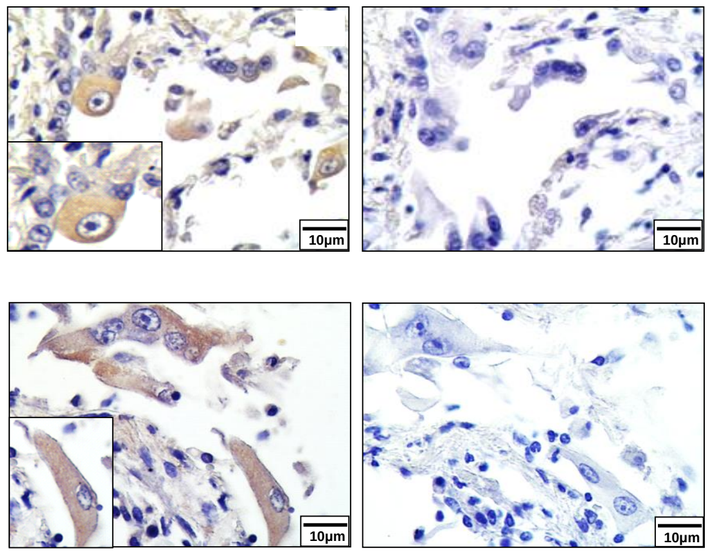

Non COVID-19 Lung

Anti-SARS-CoV-2 ab

Patient #1

Patient #2

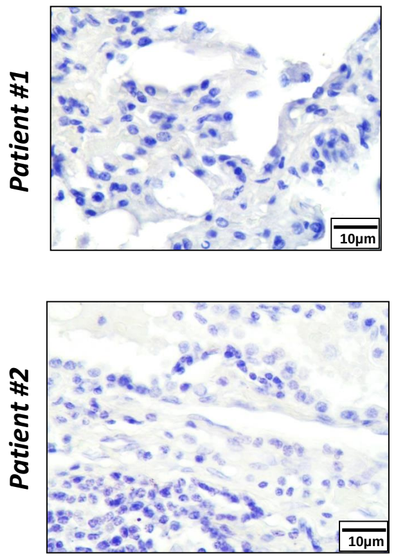

Anti-SARS-CoV-2 ab (G2 clone)

Anti-SARS-CoV-2 ab (Commercial clone1A9 Genetek)

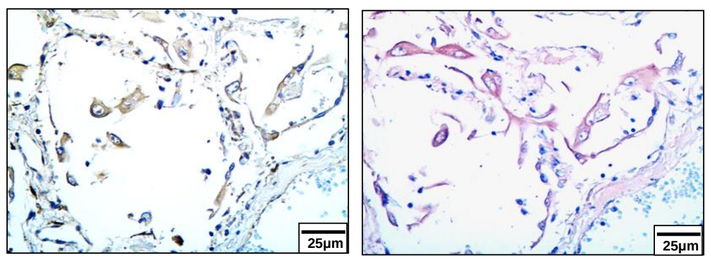

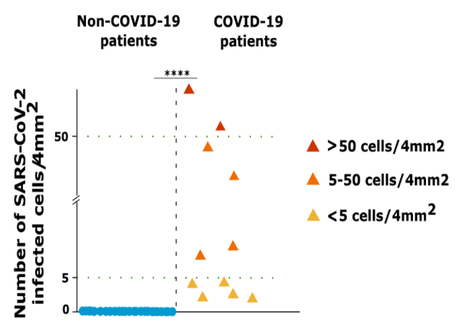

B.

COVID-19 Lung

1. Serial section analysis

Anti-SARS-CoV-2 ab

TTF-1

Anti-SARS-CoV-2 ab

ACE-2

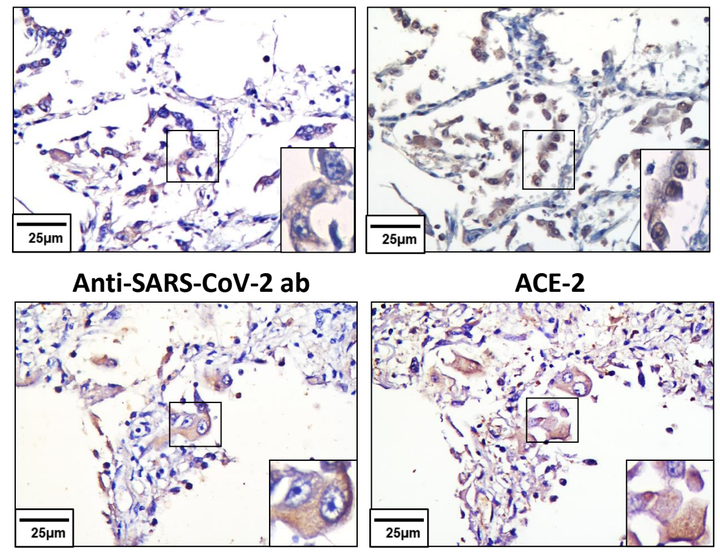

2. Double staining analysis

TTF-1 (+) / Anti-SARS-CoV-2 ab(+)

SP-B (+) / Anti-SARS-CoV-2 ab(+)

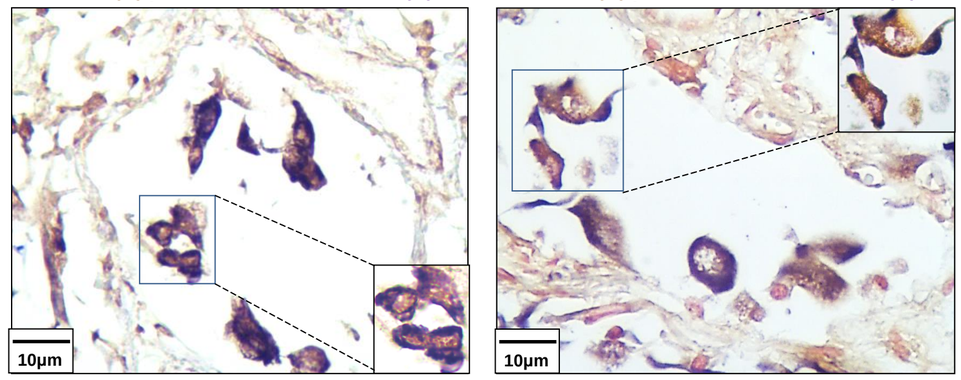

C.

COVID-19 Lung

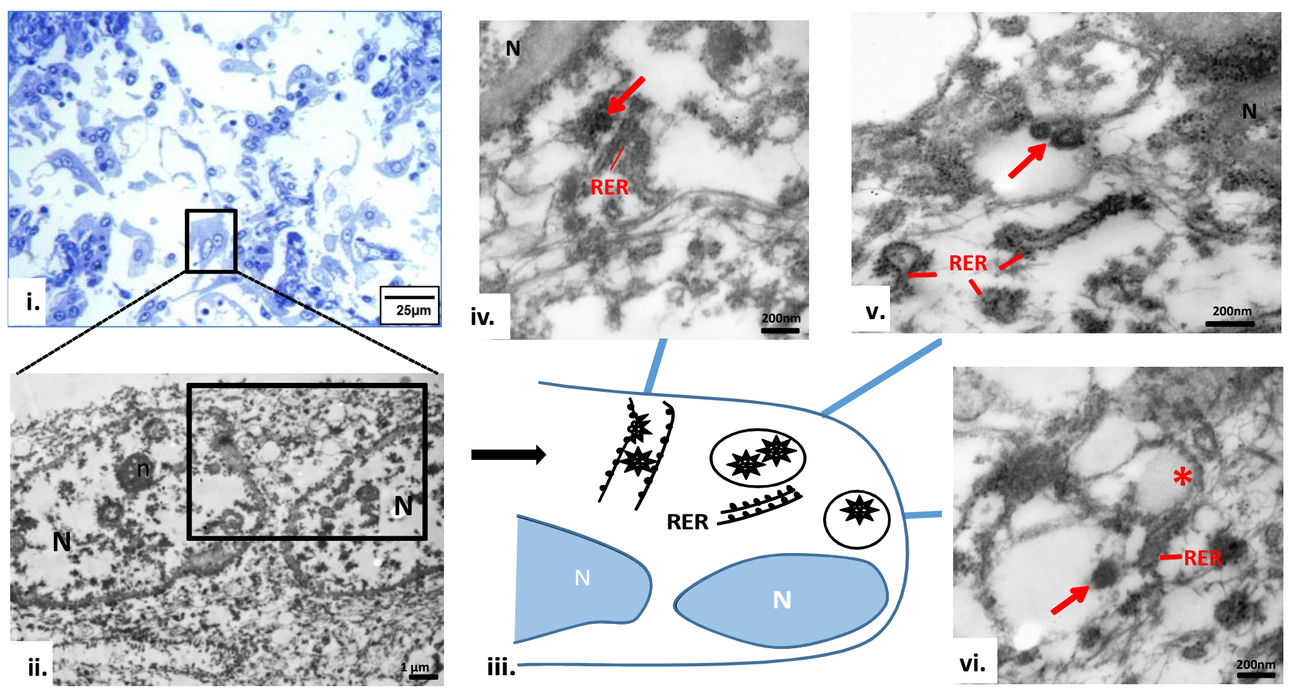

Non COVID-19 Lung

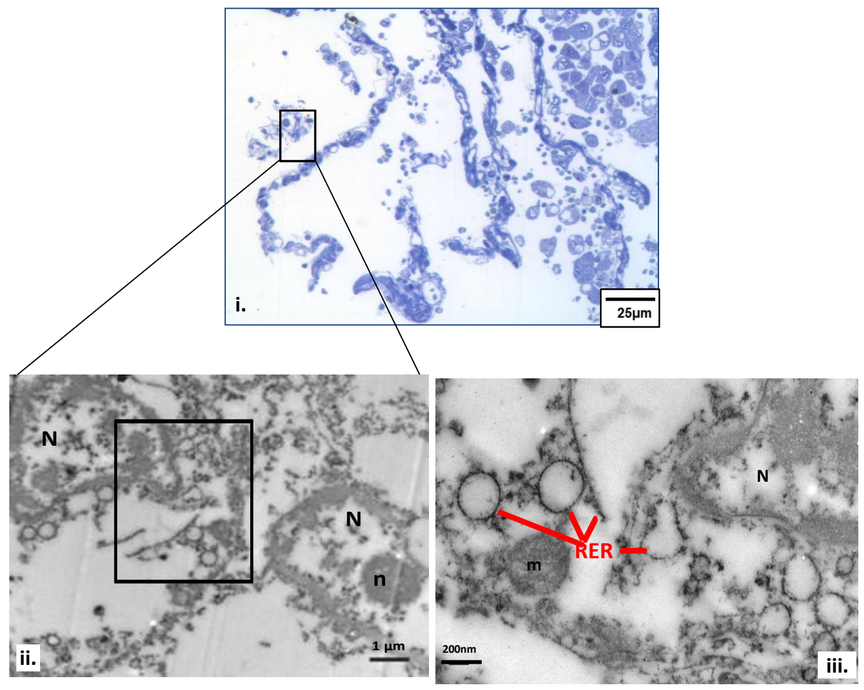

FIGURE 2.

A. COVID-19 Lung

1. Serial section analysis

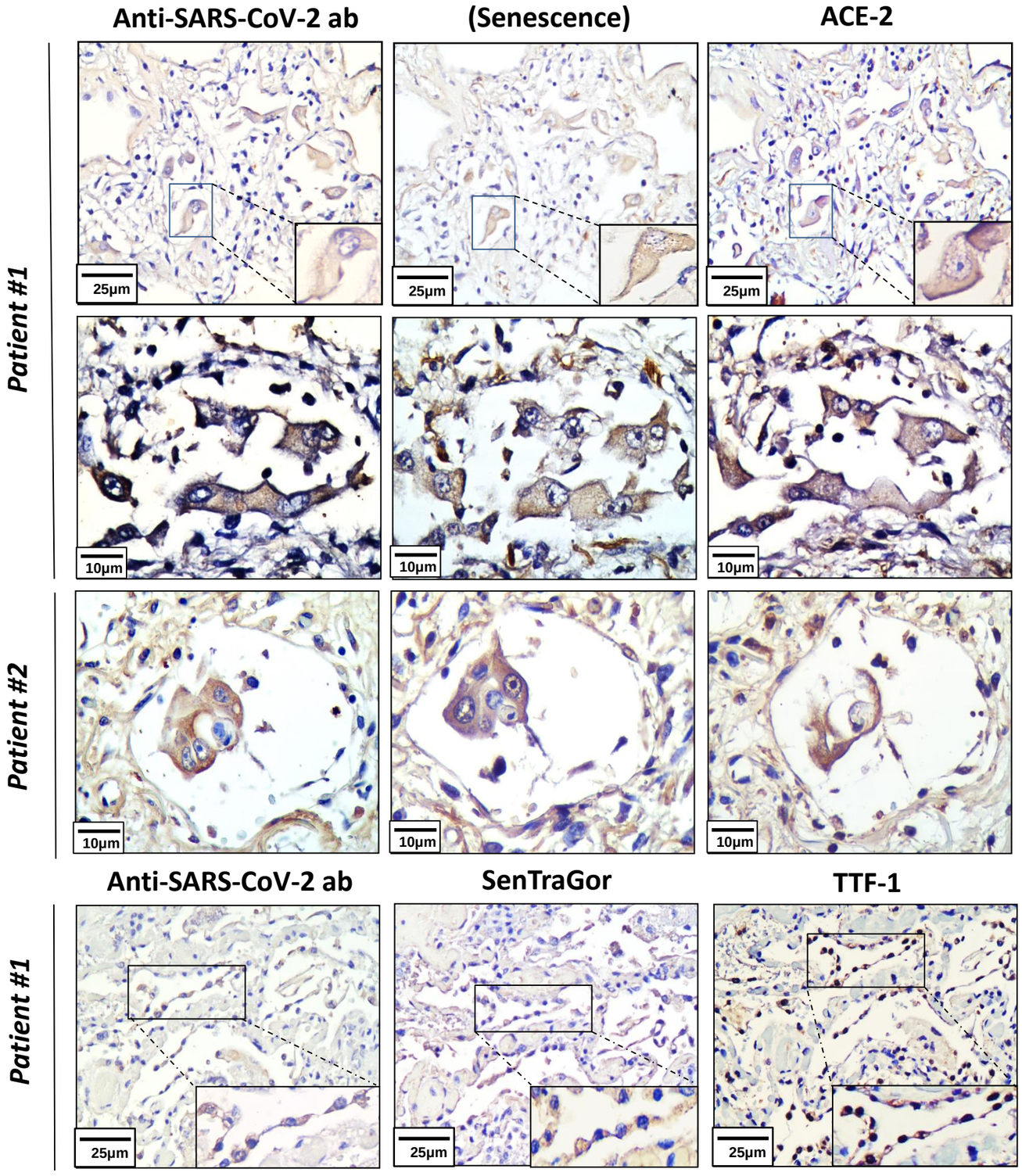

2. Double staining analysis

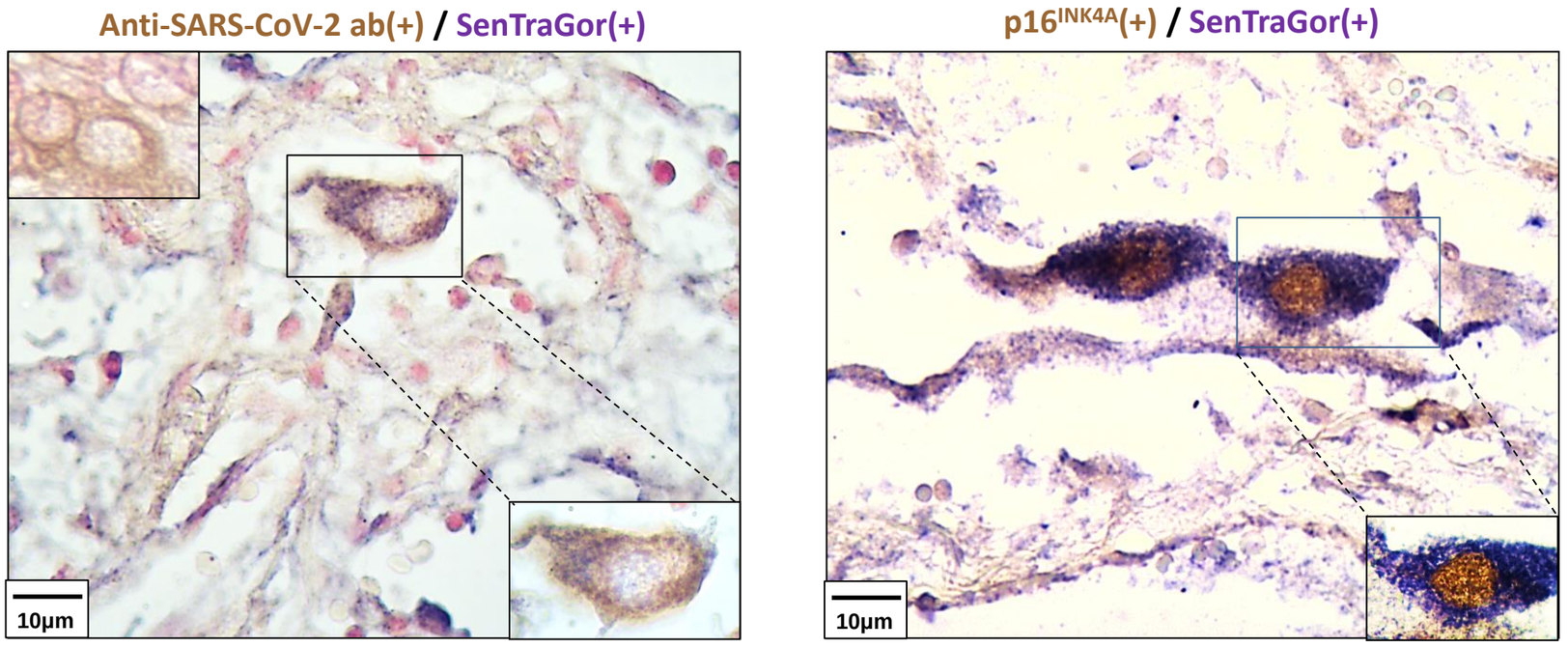

B. Non COVID-19 Lung

1. Serial section analysis

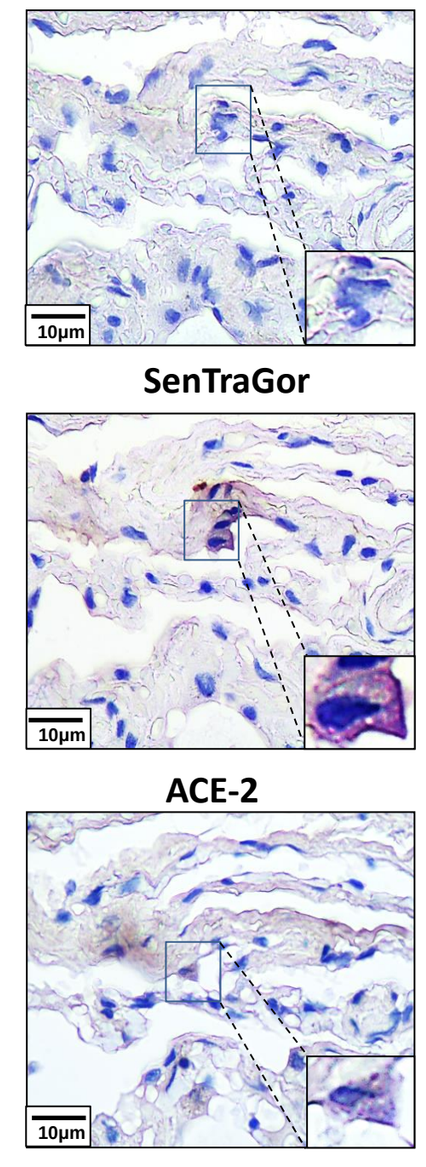

2. Double staining analysis

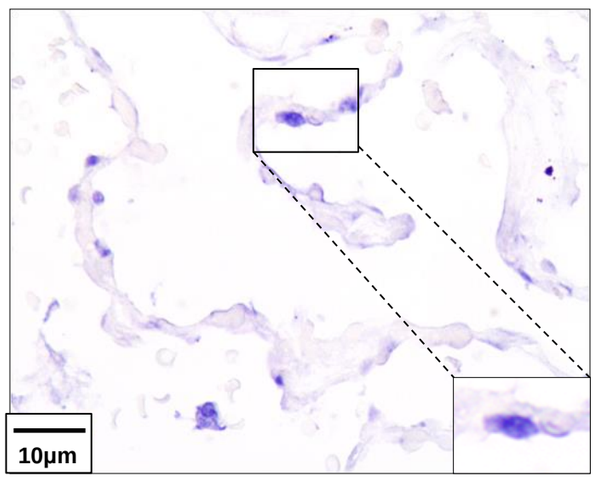

C.

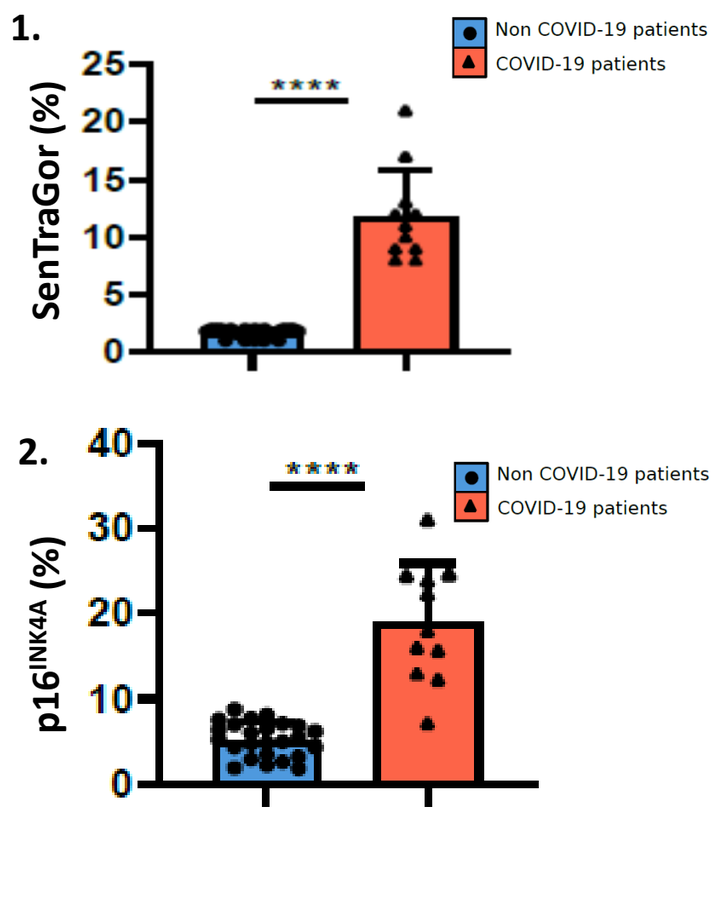

Figure 3

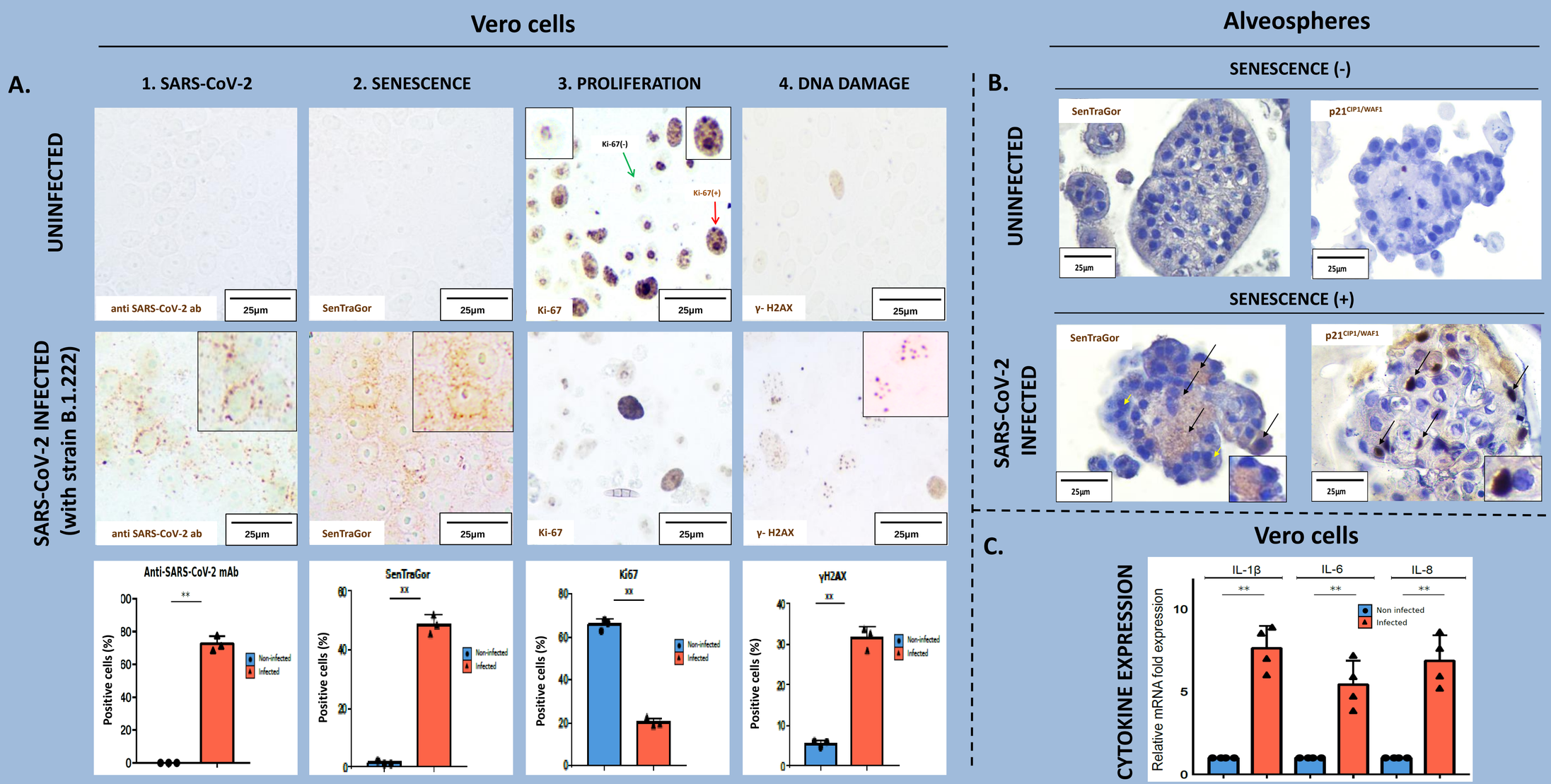
Vero cells
A.
1. SARS-CoV-2
2. SENESCENCE
3. PROLIFERATION
4. DNA DAMAGE
UNINFECTED
SARS-CoV-2 INFECTED (with strain B.1.222)
anti SARS-CoV-2 ab
SenTraGor
Ki-67
γ- H2AX
Ki-67(-)
Ki-67(+)
25µm
Anti-SARS-CoV-2 mAb
SenTraGor
Ki67
γH2AX
Positive cells (%)
Non-infected
Infected
**
xx
B.
Alveospheres
SENESCENCE (-)
SENESCENCE (+)
SenTraGor
p21CIP1/WAF1
C.
Vero cells
CYTOKINE EXPRESSION
Relative mRNA fold expression
IL-1β
IL-6
IL-8
Non infected
Infected

FIGURE 4.

A. **COVID-19 Lung**

1. Serial section analysis

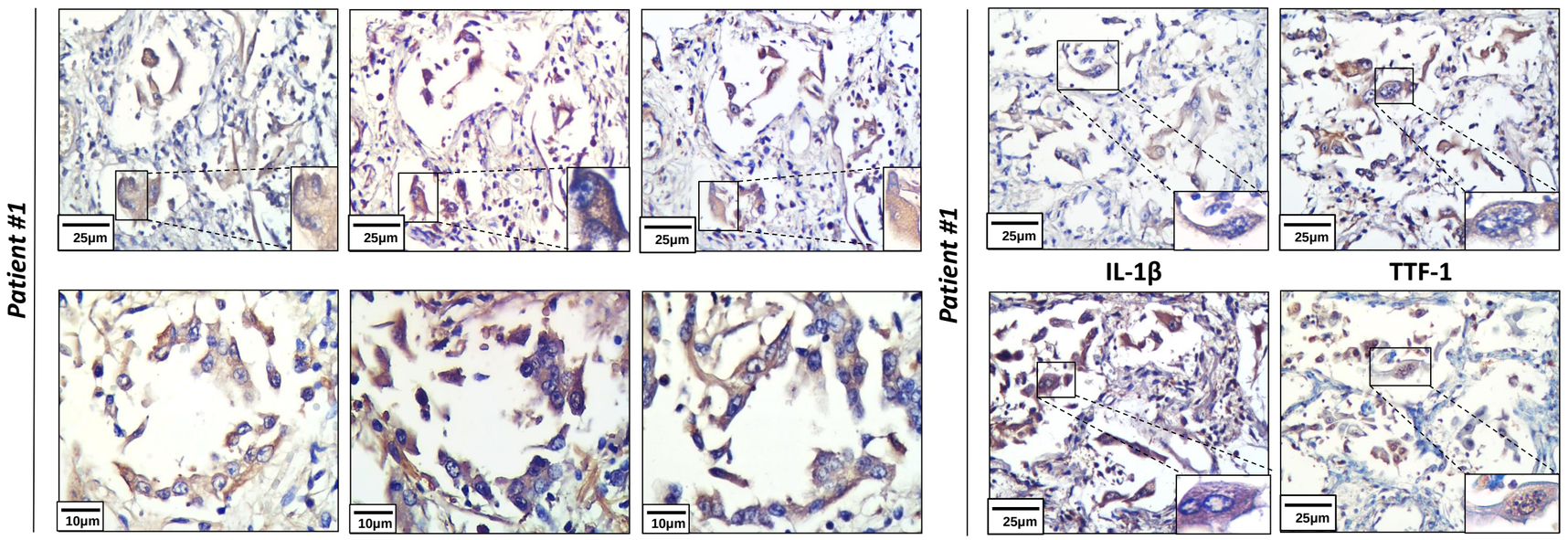

2. Double staining analysis

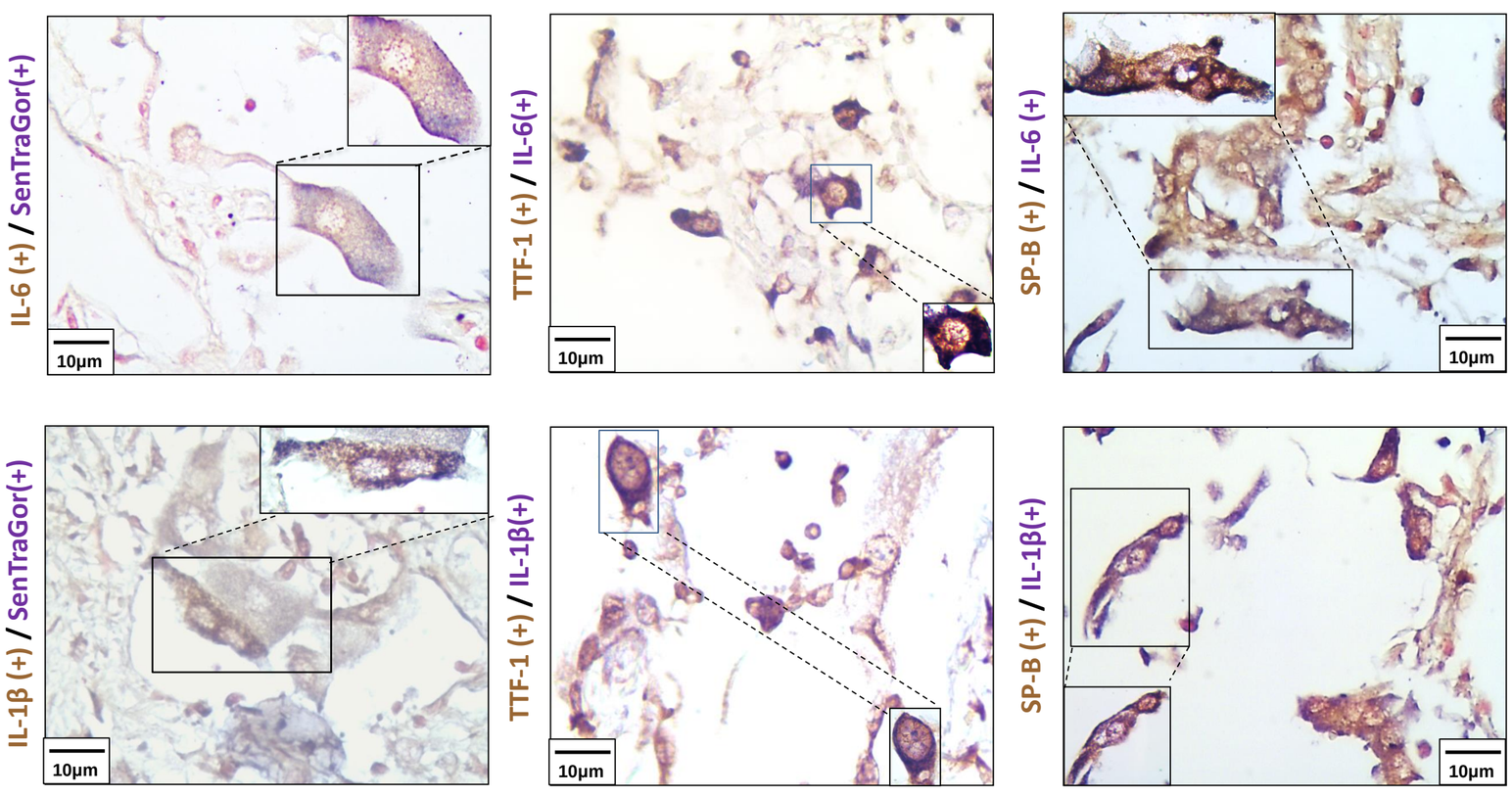

B. **Non COVID-19 Lung**

Serial section analysis

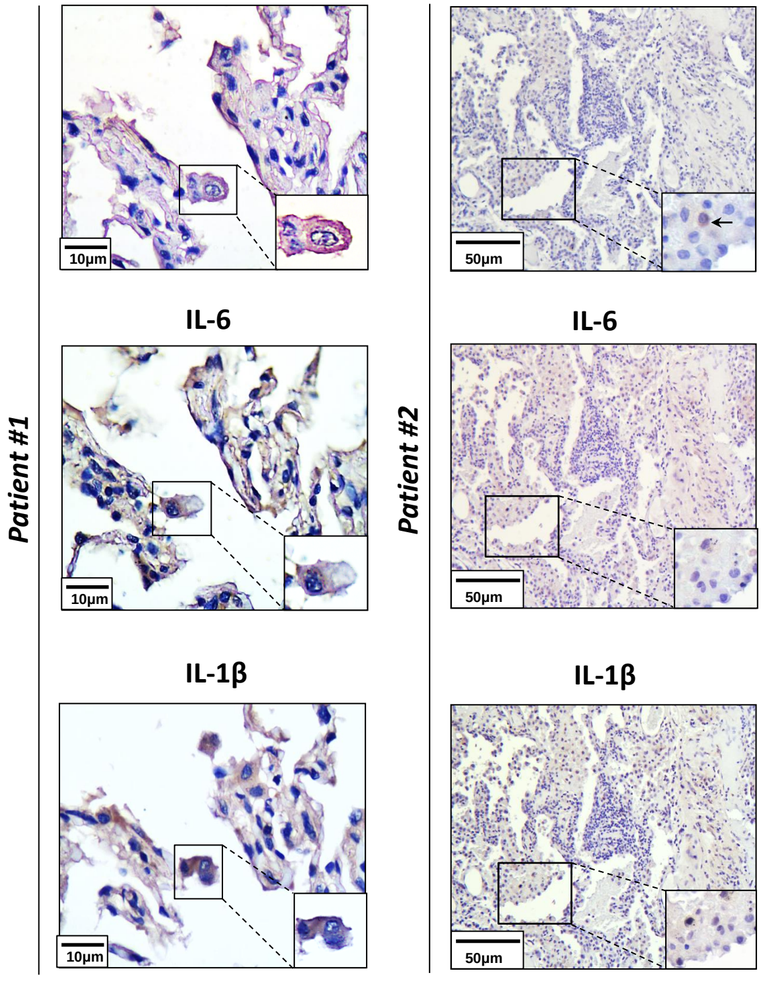

C.

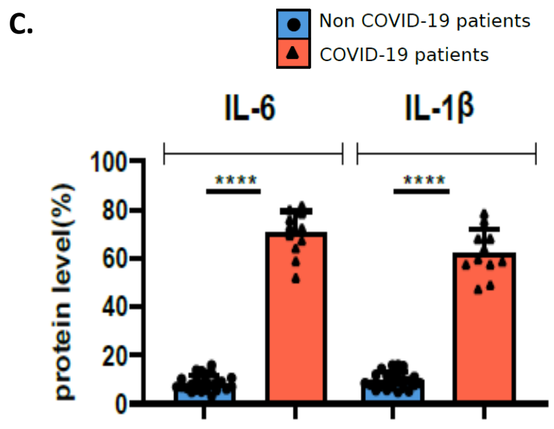

Figure 5

A.

Kidney

Non COVID-19

COVID-19

Anti-SARS-CoV-2 ab

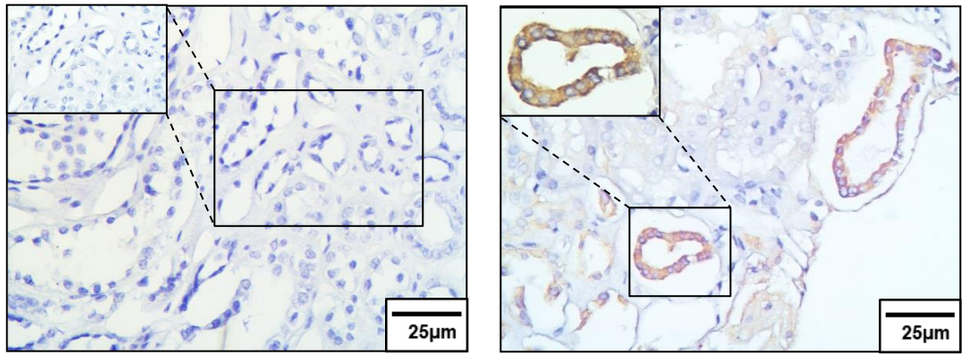

Liver

Non COVID-19

COVID-19

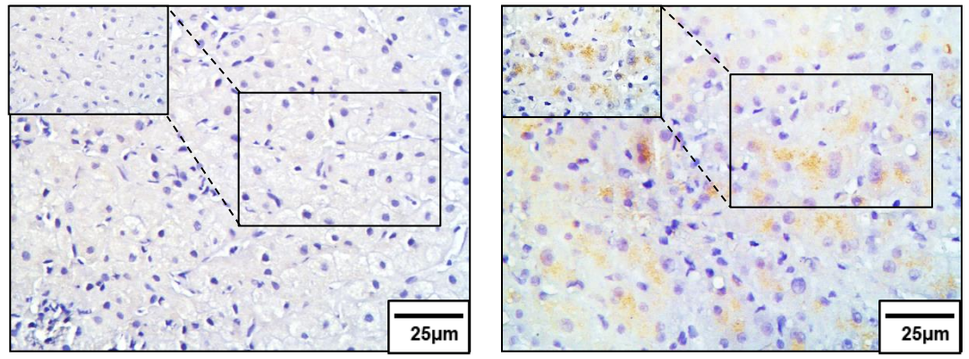

Serial section analysis in COVID-19 kidney

Anti-SARS-CoV-2 ab

G2 clone

Commercial clone 1A9 (Genetek)

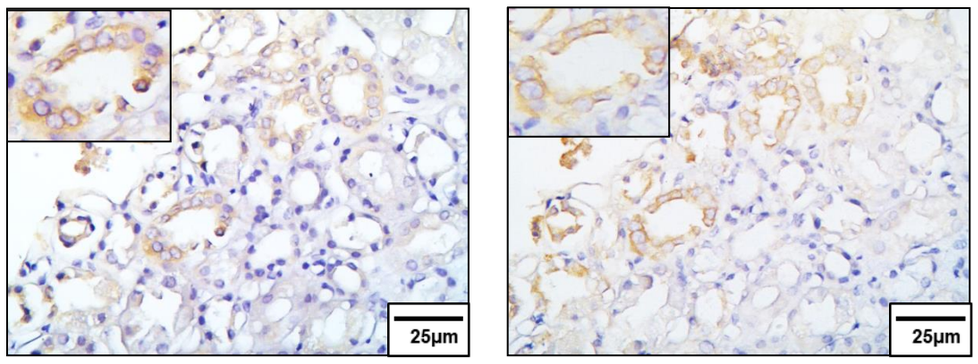

Serial section analysis in COVID-19 Liver

Anti-SARS-CoV-2 ab

G2 clone

Commercial clone 1A9 (Genetek)

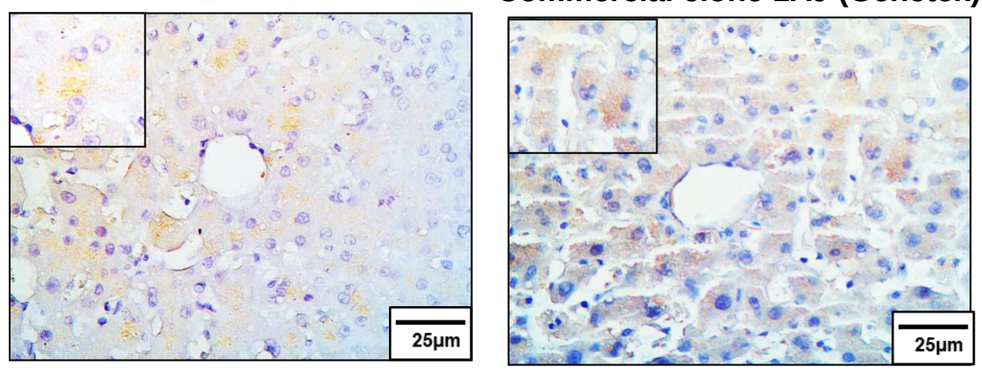

B.

COVID-19

1. Serial section analysis

Kidney

Anti-SARS-CoV-2 ab

SenTraGor

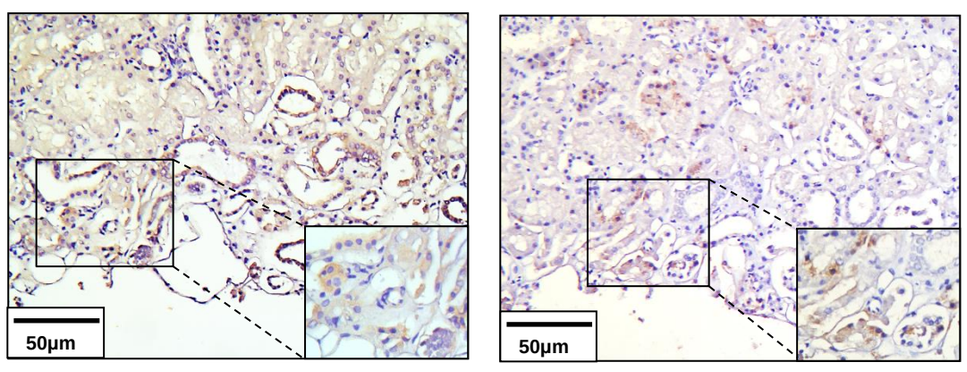

Liver

Anti-SARS-CoV-2 ab

SenTraGor

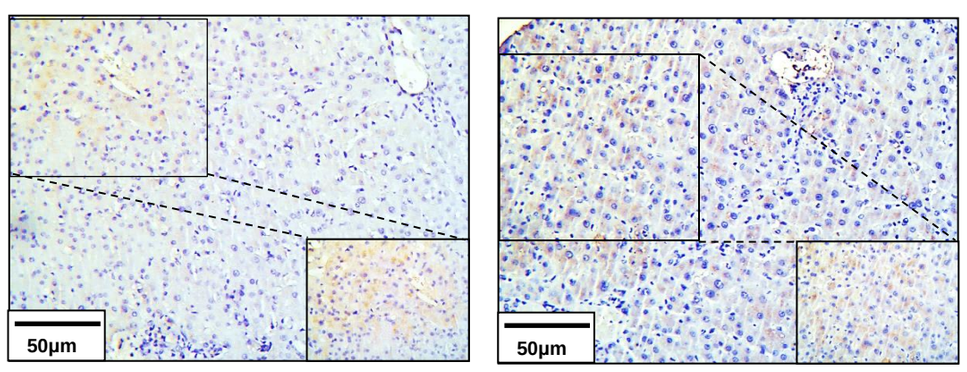

Figure 6

A. Bioinformatic screening and identification of accumulating mutations in the genome of Sars-CoV-2 isolates from patients

STEP 1. 1) Retrieve and 2) Align all viral genomes against Wuhan (NC_045512) reference genome

STEP 2. Spectrum of mutations observed

STEP 3. Frequency of mutation signatures

STEP 4. Define APOBEC sites that overlap C > U mutations

4,460,909 SARS-CoV-2 strains (deposited into:)

GISAID

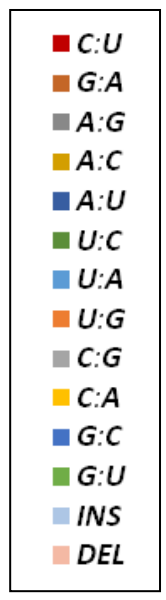

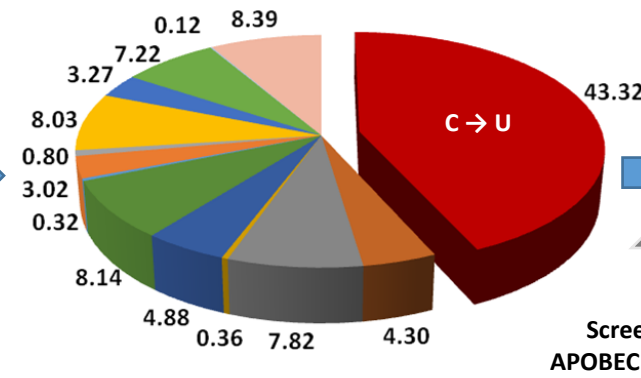

Screen using APOBEC consensus (see Fig S7 for motif generation)

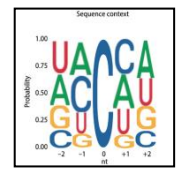

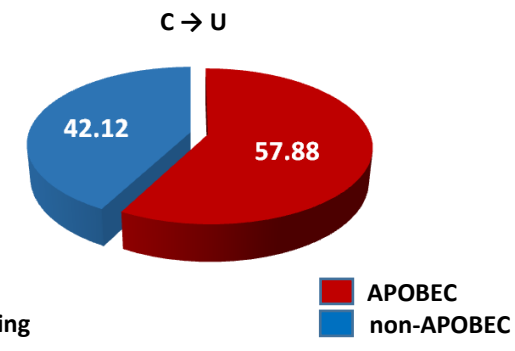

B. SARS-CoV-2 mutations acquired in senescent cells in strains isolated from patients

i. **Patient #1 (infected with strain B.1.222)**

Day 0 — Infection of VERO cells with the patient's strain

Day 17 (senescent cells) — NGS analysis of patient's strain

ii. **Patient #2 (infected with strain B.1)**

Day 0 — Infection of VERO cells with the patient's strain

Day 14 (senescent cells) — NGS analysis of patient's strain

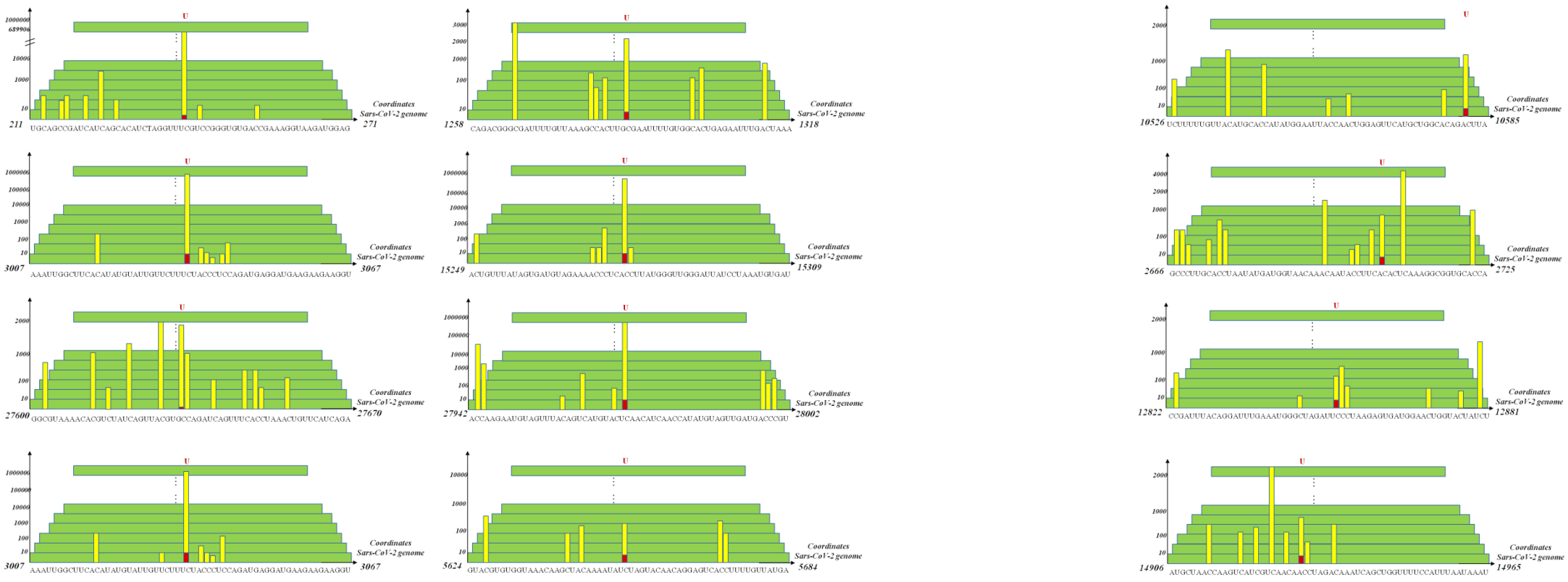

APOBEC mutations in patients-derived strains from GISAID **APOBEC mutations in strains from senescent cells (present study)** **NGS read-depth**

C.

C → U in strains from senescent cells

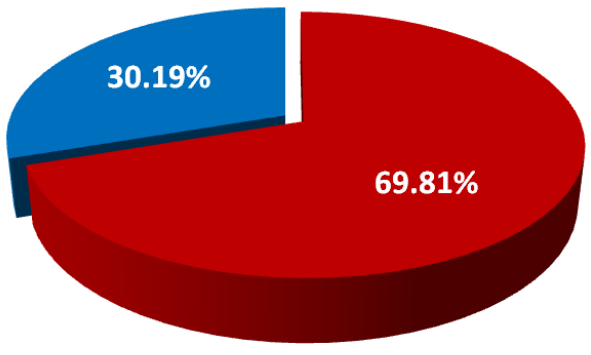

D.

Infected VERO cells

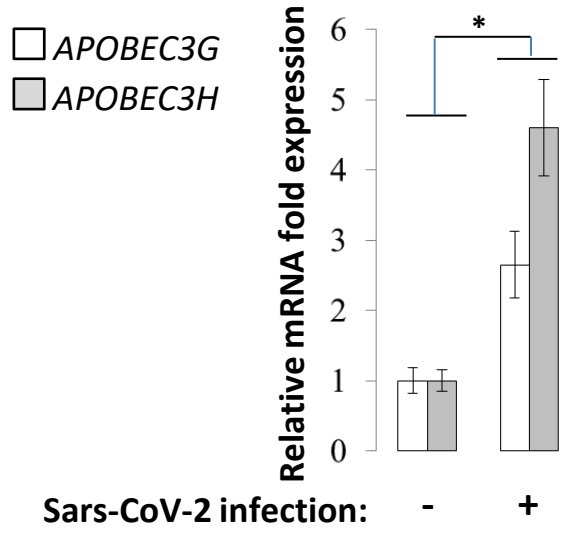

E.

Infected VERO cells

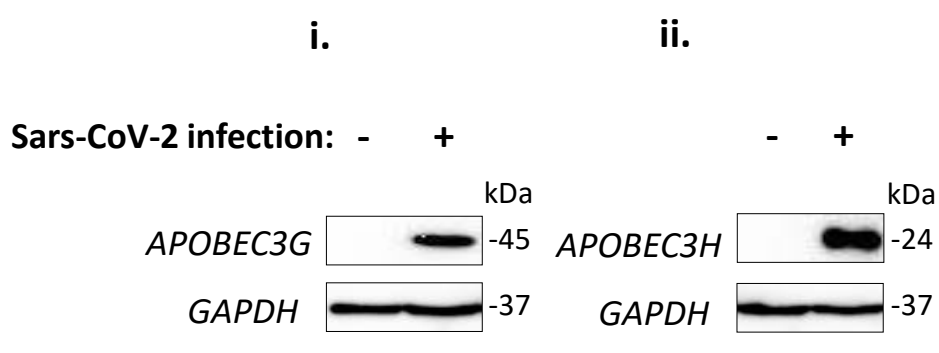

ONLINE DATA SUPPLEMENT

Material and Methods

RNA extraction and Reverse-Transcription real-time PCR (RT-qPCR) detection

SASP cytokine mRNA analysis

RNA was extracted using the Nucleospin RNA kit (Macherey-Nagel #740955) according to the manufacturer's instructions. 1 µg RNA was used for cDNA preparation with Primescript^{TM} RT Reagent Kit (Takara #RR037A). RT-qPCR was performed utilizing SYBR Select Master Mix (Life technologies #4472908) on a DNA-Engine-Opticon (MJ-Research) thermal cycler. Primer sequences employed were: IL-1β Fw: 5'-GGAAGACAAATTGCATGG-3', Rv: 5'-CCCAACTGGTACATCAGCAC-3'; IL-6 Fw: 5'- AGAGGCACTGGCAGAAAAC-3', Rv: 5'-TGCAGGAACTGGATCAGGAC-3'; IL-8 Fw: 5'-AGGACAAGAGCCAGGAAGAA-3', Rv: 5'-ACTGCACCTTCACACAGAGC-3'; B2M: β2-microglobulin (reference) gene Fw: 5'-TCTCTGGCTGGATTGGTATCT-3', Rv: 5'-CAGAATAGGCTGCTGTTCCTATC-3' [1]. Results, averaged from three independent experiments, are presented as n-fold changes after Sars-CoV-2 infection relatively to the non-infected condition, using the 2-ΔΔCT method.

Viral RNA detection

RNA was extracted using the NucleoSpin Virus RNA purification kit (Macherey-Nagel #740.983) according to the manufacturer's instructions. RT-qPCR was performed utilizing the One Step PrimeScript III RT-PCR Kit (Takara # RR601B) on a Rotor-Gene Q 6000 (Qiagen) thermal cycler following the manufacturer's instructions and using the CDC N-

gene directed primers [**https://www.cdc.gov/coronavirus/2019-ncov/lab/rt-pcr-panel-primer-probes.html**].

Next Generation Sequencing (NGS)

The Ion AmpliSeq Library Kit Plus was used to generate libraries following the manufacturer's instruction, employing the Ion AmpliSeq SARS-CoV-2 RNA custom primers panel (ID: 05280253, Thermo Fisher Scientific). Briefly, library preparation steps involved reverse transcription of RNA using the SuperScript VILO cDNA synthesis kit (Thermo Fisher Scientific), 17-19 cycles of PCR amplification, adapter ligation, library purification using the Agencourt_AMPure XP (Beckman Coulter), and library quantification using Qubit Fluorometer high-sensitivity kit. Ion 530 Chips were prepared using Ion Chef and NGS reactions were run on an Ion GeneStudio S5, ion torrent sequencer (Thermo Fisher Scientific). Samples were run in triplicates.

Protein extraction and immunoblot analysis

Total protein extracts were obtained by resuspension in 50 mM Tris/HCl pH 8.0, 150 mM NaCl, 0,1% SDS, 0,5% sodium deoxycholate, 1% NP-40 adjusted with protease and phosphatase inhibitors. Lysate was centrifuged at 13,400 rpm at 4°C for 15 min. The supernatant was collected and proteins quantified using Protein assay dye concentrate (BIO-RAD). Thirty micrograms of protein were adjusted with Laemmli buffer (Merck, 38733) and loaded on acrylamide/bis-acrylamide gels. Gel electrophoresis was followed by transfer to PVDF membrane (Macherey-Nagel, 741260), while signal development was carried out by Clarity Western ECL Substrate (Bio-Rad, 1705060) chemiluminescence and captured on an iBright CL750 Imaging System (Thermo Fisher Scientific). Horse Radish

Peroxidase conjugated anti-goat, anti-mouse and anti-rabbit secondary antibodies (1:1000 dilution) (Cell Signaling) were used. Primary antibodies were: anti-APOBEC3G/A3G (Abcam ab109727 and ab172694), anti‑APOBEC3H (LSBio LS‑C151868) and anti-GAPDH (rabbit, Cell Signaling, 2118S, 1:2000).

Anti-SARS-CoV-2 antibodies

Generation

A series of monoclonal antibodies against SARS-CoV2 Receptor Binding Domain (RBD) of spike protein were produced according to a modified method of Koehler and Milstein (Koehler and Milstein, 1975). Briefly, twelve BALB/c mice of 5 weeks of age were immunized intraperitoneally (i.p.) with 25μg of SARS-Cov2 protein (Trenzyme GmbH, Germany). All immunization and animal handling were in accordance with animal care guidelines as specified in EU Directive 2010/63/EU. After 5 cycles of immunization, mice were sacrificed, spleenocytes were collected and fused with P3X63Ag8.653 (ATCC® CRL1580™) following a modified method of Koehler and Milstein. Positive clones and antibody specificity were determined through extensive immunosorbent assays. Four clones, namely 479-S1, 480-S2, 481-S3 and 482-S4 are under patent application (Gorgoulis VG, Vassilakos D and Kastrinakis N *(2020)* GR patent application no: 22-0003846810).

RNA sequence determination and amino acid prediction

RNA was collected from biological duplicates of generated hybridomas as described elsewhere [2]. RNA samples were processed according to manufacturer's instructions, using the following kits: NEBNext® Poly(A) mRNA Magnetic Isolation Module (E7490S),

NEBNext® Multiplex Oligos for Illumina® (Index Primers Set 1, NEB7335) and NEBNext® Ultra™ II Directional RNA Library Prep with Sample Purification Beads (E7765S). After successful QC (RNA 6000 Nano bioanalyzer, Agilent) and quantity measurements (Qubit™ RNA HS Assay Kit, ThermoFisher), 1ug was used for mRNA selection, cDNA construction, adaptor ligation and PCR amplification (11 cycles), according to the manufacturer's protocol: (https://international.neb.com/products/e7760-nebnext-ultra-ii-directional-rna-library-prep-kit-for-illumina#Product%20Information). The 479-G2-ATCACG index from NEB E7335 was used. The final libraries were analyzed with Agilent High Sensitivity DNA Kit on an Agilent bioanalyzer, quantitated (Qubit dsDNA HS Assay Kit, Thermofisher) and, after multiplexing, were run using a NextSeq 500/550 Mid Output Kit v2.5 (150 cycles), paired end mode on a NextSeq550 (Illumina) at final concentration 1,3pM with 1% PhiX Control v3.

Fastq files were demultiplexed with Flexbar [3]. Quality control of the Fastq files was assessed with FastQC tools [4]. Adapter sequences were removed with Cutadapt program [5] with the following parameters: quality trimming was set to 20 and the minimum allowed nucleotide length after trimming was 20 nucleotides using --pair-filter=any to apply the filters to both paired reads. A two way alignment mode was followed to identify the antibody clone. More precisely alignments were performed with Bowtie2 [6] with parameters set as following: -D 20 -R 3 -N 1 -L 20 -i S,1,0.50 –no-mixed --no-discordant against an index made from IMGT database http://www.imgt.org/ having downloaded all mouse and human IG genes. Also this mode of alignments was executed for quality control and visualization of the aligned reads spanning the IG gene segments on the genome browser. The second mode refers to the determination and

reconstruction of the clones. This was performed with MiXCR suite [7]. At first, alignments against the IG repertoire were performed with kaligner and visualization of alignments was assessed. It was observed that the use of kaligner gave better results with higher clone hits regarding the VH and VL segments. Full assembly of the clones was performed. A full report of the number of reads and assembly of CDR and FR clones is provided in clones479_S1kalign.txt. The clones with the highest number of reads and coverage across the V, D, J segments were considered. The reported matched sequences were also checked with IgBlast tool https://www.ncbi.nlm.nih.gov/igblast/. In addition, after the assembly of the amino acid reconstruction of the FR and CDR regions of the full variable fragment for both the Heavy and Light antibody chains, a 3D visualization was also determined via folding the V protein fragment with iTassser suite [8]. The above analysis has been extensively described in Gorgoulis VG, Vassilakos D and Kastrinakis N. *(2020)* GR patent application no: 22-0003846810.

Immunocytochemistry (ICC)-Immunohistochemistry (IHC)

Method: ICC and IHC were performed according to previous published protocols [9]. In brief, 3 μm thick sections from formalin-fixed paraffin embedded (FFPE) lung tissues were employed. Antigen retrieval was heat-mediated in 10 mM citric acid (pH 6.0) for 15-20 minutes. The following primary antibodies were applied: i) the anti-SARS-CoV-2 (G2) monoclonal antibody (dilution 1:300), ii) anti-SARS-CoV-2 mononclonal antibody [1A9 clone Genetek, Cat.no: GTX632604 (dilution 1:100], iii) anti-ACE-2 [Rabbit polyclonal antibody Abcam, Cat.no: ab15348 (dilution 1:200)], iv) anti-TTF-1 [mouse monoclonal antibody Dako, Clone 8G7G3/1, Cat.no: M3575 (Ready-to-Use)], v) anti-Surfactant Protein B (SP-B) [1B9 clone ZETA Corporation Cat.no: Z2196ML (dilution 1: 100)], vi) anti-

$p16^{INK4A}$ [mouse monoclonal antibody Santa Cruz, clone: F-12, Cat.no.:sc-1661. (dilution 1:100)], vii) IL-1β [Rabbit polyclonal antibody Abcam, Cat.no: ab2105 (dilution 1:150)], viii) IL-6 [mouse monoclonal antibody R&D systems, clone: Clone: 6708, Cat.no:MAB206 (dilution 1:100)], ix) anti-γH2AX [Phospho-Histone H2A.X (Ser139) clone:(20E3) Rabbit cat.no.:mAb #9718 dilution: 1/400] and x) anti-Ki67 [clone: SP6 cat.no.: ab16667 dilution: 1/250], anti- $p21^{WAF1/CiIP1}$ [clone: 12D1 Rabbit cat.no.: mAb #2947 dilution 1/100], all overnight at 4^{o}C. Development of the signal was achieved using the Novolink Polymer Detection System (Cat.no: RE7150-K, Leica Biosystems). Specimens were counterstained with hematoxylin.

Negative Controls for the anti-SARS-CoV-2 (G2) monoclonal antibody: *i) Biological,* comprising previously published and new lung tissue samples from a cohort of 60 cases that underwent surgery prior to COVID-19 outbreak [10]. *ii) Technical:* a. Omission of the G2 primary monoclonal antibody, b. Blocking of the G2 primary monoclonal antibody using the corresponding S-protein (Cat.no. P2020-029, Trenzyme) in a 1:10 (G2/Spike protein) ratio and c. Two slides per case were employed for each staining or control experiment.

Evaluation of G2 staining: Cells were considered positive irrespective of the staining intensity. Two different semi-quantitative IHC evaluation approaches, previously described were adopted [11, 12] According to the first, the number of G2 positive cells per $4mm^2$ was encountered and scored according to the following criteria: (+) for positive staining in <5 cells per 4 mm^2, (++) for positive staining in 5–50 cells per $4mm^2$ and (+++) for positive staining in >50 cells per 4 mm^2 [10]. Regarding the second one, the number of G2 positive cells per whole slide was estimated and subsequent scores were assessed: (+) between one and five positive cells per whole slide (scattered cells), (++) more than

five cells per whole slide but no foci (isolated cells) and (+++) more than 10 cells in one × 20 field (with foci) [11]. For $p16^{INK4A,}$ the mean percentage of positive alveolar cells in at least 10 high power fields (x400) per patient was measured. This information has been included in the methods section (Main and Online Suppl Data). For IL-6 and IL-1b, the percentage of immunopositive cells was encountered [13]. Evaluations were performed blindly by four experienced pathologists (KE, PF, CK and VG) and intra-observer variability was minimal ($p \leq 0.05$).

Bioinformatic analysis for identification of mutational signatures in the SARS-CoV-2 genome

Screening for mutational signatures in the SARS-CoV-2 genome

To investigate the mutational patterns of the SARS-CoV-2 genome we downloaded from GISAID database (https://www.gisaid.org/) 4,672,296 available strains that were distributed globally (*Step 1* in **Figure S7**). These strains were aligned with Bowtie aligner [6], having as reference the Wuhan first assembly NC_045512, obtained from NCBI (https://www.ncbi.nlm.nih.gov/sars-cov-2/) (*Step 2* in **Figure S7**). More information regarding the commands used for the alignments is provided in Part 1 of the supplementary code file (bioinformatic.analysis.sh). The identification of mutations is performed with an "in-house" script (Part 2 of supplementary code file) using calmd function from SAMtools [14], which is based on proteome occupancy profile studies (*Step 3* in **Figure S7**) [15]. Candidate APOBEC sites need to have a C→U frequency of mutation at the same nucleotide position of more than 5 reads. Furthermore, in order to investigate at RNA secondary structure level the filtered deaminated sites (with more than 5 C→U mutation counts), we extracted windows of ±60 nucleotides around the

C→U most frequent sites and interrogated the folding of the RNA sequences using the Vienna RNA fold algorithm (*Step 4* in **Figure S7**) [16]. To guide the RNA folding we incorporated SHAPE reactivities from SHAPE-seq data for SARS-CoV-2 [17]. To decipher the candidate motifs we counted the frequency of letters starting from k-mers of ±5 nucleotides from the most frequent deaminated position up to 30-mers, which is usually taken as an upper limit in most RBP pull-downs and usually corresponds to the protein bound protected fragment [18, 19] (*Step 4* in **Figure S7**). The frequency for each letter was determined via a perl script, which extracts all possible k-mers and their frequencies. The highest motif consensus was around ±5 nucleotides from the C→U deaminated nucleotide, as the motif becomes more degenerate when extending above ±7 nucleotides. Next, the frequency of each k-mer was plotted with Web-logo motifs [20]. In addition position-weight matrices (PWM) for each letter (nucleotide) around the deaminated RNA nucleotides were extracted. A Markov model which extracts the probability of each pairs of nucleotide in each position of the k-mer was also used (i.e. frequency of Adenine in position 1 of the 5mer (A_1) followed by C at position 2, followed by U at position 3), thus a score k-mer matrix is formed demonstrating the probability of each nucleotide per position plus the probability of having specific pairs of di-nucleotides (*Step 4*, right hand panel, in **Figure S7**). The dominant RNA structure motif was identified using the BEAM software [21]. Overall the motif analysis regarding the sequence composition around the most frequently deaminated sites, along with the RNA structure, revealed an UACCA enrichment around regions of open hairpin structures, in agreement with the results from the literature [22-27].

Filtering and alignments of Fastq files

Filtering and alignments of Fastq files for the SARS-CoV2 strains from the infected Vero E6 cells and from actual patients were demultiplexed with Flexbar [3]. Quality control of the Fastq files was assessed with FastQC tools [4]. Adapter sequences were removed with Cutadapt program [5] with the following parameters: quality trimming was set to 28 and the minimum allowed nucleotide length after trimming was 21 nucleotides. Potential, very high over-represented k-mers, at the beginning of the reads, were removed. Alignments were performed with Bowtie2 [6] with the parameter –very-sensitive using as a reference genome the B.1.222 and the B.1 (accession No MT459880.1) SARS-CoV2 strains.

Mutation analysis of other viruses

Data for HIV, HPV, KSHV, and EBV virus strains were downloaded from NCB1 virus (https://www.ncbi.nlm.nih.gov/labs/virus/vssi/#/). Alignments for each virus strain were performed by applying Bowtie 2 [6] and using the following as reference genomes: NC_001802.1 for HIV, NC_009333.1for HPV, NC_009333.1 for KSHV and NC_009334.1 for EBV. Alignments in Bowtie 2 were carried out setting the parameter –very-sensitive. The different strains examined for HIV were 482, 100 for HPV, 12 for KSHV and 15 for EBV. Mutational status analysis for each virus was performed similarly to that followed for APOBEC identification and is explained i**n Step1** of the supplementary code file (bioinformatic.analysis.sh). The identification of mutations was performed with the "in-house" script (**Step 2** of supplementary code file) using in parallel calmd function from SAMtools [14]. The number of mutations observed in the different strains versus the total captured sequenced bases for each of the strains, was plotted for each virus, using

boxplots in R. Statistical significance was determined by applying Wilcoxon rank-sum test with the symbol ** corresponding to statistical significance of p-value<=0.01.

Suppl Figure Legends

Figure S1: SARS-CoV-2 antibody production and screening selection. A. Workflow of the procedure for antibody production. **B.** Sequel of screening steps for antibody production and selection. **C.** Final screening step processes leading to the selection of G2 monoclonal antibody. Graph depicting the structure of G2 antibody as well as the DNA sequences of FRs and CDRs elements of variable regions.

Figure S2: G2 immunostaining in COVID-19 lungs. Representative immunohistochemical results depicting G2 positive and negative staining in small peripheral airways of COVID-19 lungs.

Figure S3: Quantification of double anti-SARS-CoV-2 ab (G2)/SenTraGor and anti-SARS-CoV-2 ab (G2)/p16 positive AT-II cells in non COVID19 and COVID19 lung parenchyma. ****p<0.001

Figure S4: Immunohistochemcal analysis in acute non COVID-19 pneumonias. Representative images from serial section staining of anti-SARS-CoV-2 ab G2, SenTraGor, ACE-2, TTF-1, IL-6, IL1-β and $p16^{INK4a}$ in the lung parenchyma from acute non COVID-19 pneumonia cases (**A**) and corresponding statistical analysis (**B**). ****p<0.001

Figure S5: SARS-CoV-2 induced senescence in Vero cells (**A) and in the alveospheres (B).** Double immunostaining for SARS-CoV-2 infection/senescence induction (1), senescence induction/cellular proliferation (2) and senescence induction (3). B. Staining for

senescence induction (assessed by SenTraGor) in the alveospheres shown in Figure 3. Black arrows depict senescent cells in comparison to non senescent ones (yellow arrow). Absence of senescence is clearly evident in non infected alveolar cells.

Figure S6: ATM inhibition in Infected Vero E6 cells results in senescence suppression. Treated, with the ATM inhibitor KU-55933, Vero cells exhibit dramatic decrease in senescence assessed by SenTraGor staining (graph, $p<0.0001$).

Figure S7: Flow diagram of bioinformatic steps followed for the identification of APOBEC mutational signatures in the SARS-CoV-2 genome. From GISAID database (https://www.gisaid.org/) 4,672,296 available strains were downloaded (Step 1), aligned against the Wuhan first assembly NC_045512 (https://www.ncbi.nlm.nih.gov/sars-cov-2/) as reference (Step 2), and mutations were identified followed by recall of C→U mutation with >5 NGS read depths (Step 3). Flanking sequences (*k-mers*) around the recorded C→U mutations were interrogated at linear and secondary conformation (2D) level (see online supplemental Materials and Methods for details) and verified against experimentally validated APOBEC motifs to confirm C→U substitutions that are APOBEC-mediated. NGS: Next Generation Sequencing.

Figure S8: Hypothetical model: Features and mechanistic insights of SARS-CoV-2 induced senescence. Briefly, SARS-CoV-2 entrance results in activation of stress response signaling pathways. The virus hijacks certain cellular functions linked with RNA processing, translation and endoplasmic reticulum turnover causing increased energy

consumption and eventually an energy shift. Increased ROS production and oxidative stress lead to DNA damage and DNA damage response activation. In addition, DDR and the subsequent cell cycle arrest is also driven by an interaction of Coronavirus nsp13 protein and DNA polymerase δ and SASP via the cGAS/STING and other DNA damage dependent pathways.

Figure S9: APOBEC-mediated mutations in the genome of the omicron (B.1.1.529) SARS-CoV-2 variant of concern. Histogram depicts the predominance of C→U substitutions in the genome of omicron strains deposited in the GISAID database. The majority of these mutations are APOBEC derived (pie chart), following application of the algorithm of Figure S7.

Figure S10: Differences in mutation rates between viruses inducing and bypassing senescence. Box plots depicting that viruses bypassing senescence exhibit significantly lower mutation rates in comparison to viruses inducing senescence. **p<0.01

Suppl Table 1: Clinicopathological characteristics of COVID-19 and non-COVID control cases examined for G2 antibody, senescence, IL-6 and IL-1b, and evaluation results in the corresponding lung tissues.

References

1. Huan CC, Wang HX, Sheng XX, Wang R, Wang X, Liao Y, Liu QF, Tong GZ, Ding C, Fan HJ, Wu JQ, Mao X. Porcine epidemic diarrhea virus nucleoprotein contributes to HMGB1 transcription and release by interacting with C/EBP-β. *Oncotarget* 2016: 7(46): 75064-75080.
2. Komseli ES, Pateras IS, Krejsgaard T, Stawiski K, Rizou SV, Polyzos A, Roumelioti FM, Chiourea M, Mourkioti I, Paparouna E, Zampetidis CP, Gumeni S, Trougakos IP, Pefani DE, O'Neill E, Gagos S, Eliopoulos AG, Fendler W, Chowdhury D, Bartek J, Gorgoulis VG. A prototypical non-malignant epithelial model to study genome dynamics and concurrently monitor micro-RNAs and proteins in situ during oncogene-induced senescence. *BMC genomics* 2018: 19(1): 37.
3. Dodt M, Roehr JT, Ahmed R, Dieterich C. FLEXBAR-Flexible Barcode and Adapter Processing for Next-Generation Sequencing Platforms. *Biology* 2012: 1(3): 895-905.
4. Andrews S. FastQC: a quality control tool for high throughput sequence data. http://www.bioinformatics.babraham.ac.uk/projects/fastqc, 2010.
5. Martin M. Cutadapt removes adapter sequences from high-throughput sequencing reads. *2011* 2011: 17(1): 3.
6. Langmead B, Salzberg SL. Fast gapped-read alignment with Bowtie 2. *Nat Methods* 2012: 9(4): 357-359.
7. Bolotin DA, Poslavsky S, Davydov AN, Frenkel FE, Fanchi L, Zolotareva OI, Hemmers S, Putintseva EV, Obraztsova AS, Shugay M, Ataullakhanov RI, Rudensky AY, Schumacher TN, Chudakov DM. Antigen receptor repertoire profiling from RNA-seq data. *Nature biotechnology* 2017: 35(10): 908-911.
8. Yang J, Yan R, Roy A, Xu D, Poisson J, Zhang Y. The I-TASSER Suite: protein structure and function prediction. *Nat Methods* 2015: 12(1): 7-8.
9. Evangelou K, Lougiakis N, Rizou SV, Kotsinas A, Kletsas D, Muñoz-Espín D, Kastrinakis NG, Pouli N, Marakos P, Townsend P, Serrano M, Bartek J, Gorgoulis VG. Robust, universal biomarker assay to detect senescent cells in biological specimens. *Aging cell* 2017: 16(1): 192-197.
10. Gorgoulis VG, Vassiliou LV, Karakaidos P, Zacharatos P, Kotsinas A, Liloglou T, Venere M, Ditullio RA, Jr., Kastrinakis NG, Levy B, Kletsas D, Yoneta A, Herlyn M, Kittas C, Halazonetis TD. Activation of the DNA damage checkpoint and genomic instability in human precancerous lesions. *Nature* 2005: 434(7035): 907-913.
11. Schaefer IM, Padera RF, Solomon IH, Kanjilal S, Hammer MM, Hornick JL, Sholl LM. In situ detection of SARS-CoV-2 in lungs and airways of patients with COVID-19. *Modern pathology : an official journal of the United States and Canadian Academy of Pathology, Inc* 2020: 33(11): 2104-2114.
12. Remmelink M, De Mendonça R, D'Haene N, De Clercq S, Verocq C, Lebrun L, Lavis P, Racu ML, Trépant AL, Maris C, Rorive S, Goffard JC, De Witte O, Peluso L, Vincent JL, Decaestecker C, Taccone FS, Salmon I. Unspecific post-mortem findings despite multiorgan viral spread in COVID-19 patients. *Critical care (London, England)* 2020: 24(1): 495.
13. van Vliet T, Varela-Eirin M, Wang B, Borghesan M, Brandenburg SM, Franzin R, Evangelou K, Seelen M, Gorgoulis V, Demaria M. Physiological hypoxia restrains the senescence-associated secretory phenotype via AMPK-mediated mTOR suppression. *Molecular cell* 2021: 81(9): 2041-2052.e2046.
14. Li H, Handsaker B, Wysoker A, Fennell T, Ruan J, Homer N, Marth G, Abecasis G, Durbin R. The Sequence Alignment/Map format and SAMtools. *Bioinformatics* 2009: 25(16): 2078-2079.
15. Schueler M, Munschauer M, Gregersen LH, Finzel A, Loewer A, Chen W, Landthaler M, Dieterich C. Differential protein occupancy profiling of the mRNA transcriptome. *Genome Biol* 2014: 15(1): R15.
16. Gruber AR, Lorenz R, Bernhart SH, Neuböck R, Hofacker IL. The Vienna RNA websuite. *Nucleic Acids Res* 2008: 36(Web Server issue): W70-74.

17. Manfredonia I, Nithin C, Ponce-Salvatierra A, Ghosh P, Wirecki TK, Marinus T, Ogando NS, Snijder EJ, van Hemert MJ, Bujnicki JM, Incarnato D. Genome-wide mapping of SARS-CoV-2 RNA structures identifies therapeutically-relevant elements. *Nucleic Acids Res* 2020: 48(22): 12436-12452.
18. Hafner M, Katsantoni M, Köster T, Marks J, Mukherjee J, Staiger D, Ule J, Zavolan M. CLIP and complementary methods. *Nature Reviews Methods Primers* 2021: 1(1): 20.
19. Van Nostrand EL, Freese P, Pratt GA, Wang X, Wei X, Xiao R, Blue SM, Chen JY, Cody NAL, Dominguez D, Olson S, Sundararaman B, Zhan L, Bazile C, Bouvrette LPB, Bergalet J, Duff MO, Garcia KE, Gelboin-Burkhart C, Hochman M, Lambert NJ, Li H, McGurk MP, Nguyen TB, Palden T, Rabano I, Sathe S, Stanton R, Su A, Wang R, Yee BA, Zhou B, Louie AL, Aigner S, Fu XD, Lécuyer E, Burge CB, Graveley BR, Yeo GW. A large-scale binding and functional map of human RNA-binding proteins. *Nature* 2020: 583(7818): 711-719.
20. Crooks GE, Hon G, Chandonia JM, Brenner SE. WebLogo: a sequence logo generator. *Genome Res* 2004: 14(6): 1188-1190.
21. Pietrosanto M, Mattei E, Helmer-Citterich M, Ferrè F. A novel method for the identification of conserved structural patterns in RNA: From small scale to high-throughput applications. *Nucleic Acids Res* 2016: 44(18): 8600-8609.
22. Maiti A, Myint W, Kanai T, Delviks-Frankenberry K, Sierra Rodriguez C, Pathak VK, Schiffer CA, Matsuo H. Crystal structure of the catalytic domain of HIV-1 restriction factor APOBEC3G in complex with ssDNA. *Nat Commun* 2018: 9(1): 2460.
23. Sharma S, Patnaik SK, Taggart RT, Baysal BE. The double-domain cytidine deaminase APOBEC3G is a cellular site-specific RNA editing enzyme. *Scientific reports* 2016: 6: 39100.
24. Sharma S, Baysal BE. Stem-loop structure preference for site-specific RNA editing by APOBEC3A and APOBEC3G. *PeerJ* 2017: 5: e4136.
25. Di Giorgio S, Martignano F, Torcia MG, Mattiuz G, Conticello SG. Evidence for host-dependent RNA editing in the transcriptome of SARS-CoV-2. *Sci Adv* 2020: 6(25): eabb5813.
26. Pan Y, Sun Z, Maiti A, Kanai T, Matsuo H, Li M, Harris RS, Shlyakhtenko LS, Lyubchenko YL. Nanoscale Characterization of Interaction of APOBEC3G with RNA. *Biochemistry* 2017: 56(10): 1473-1481.
27. Olson ME, Harris RS, Harki DA. APOBEC Enzymes as Targets for Virus and Cancer Therapy. *Cell Chem Biol* 2018: 25(1): 36-49.

Suppl Figure 1

A.

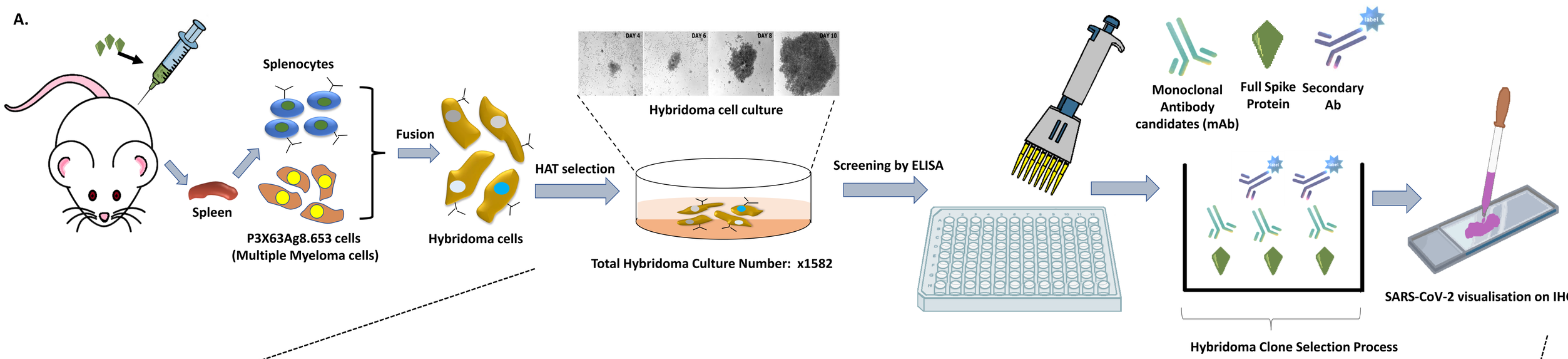

B.

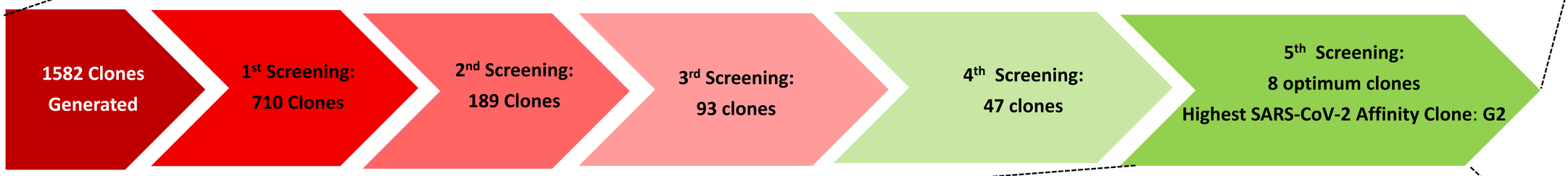

C.

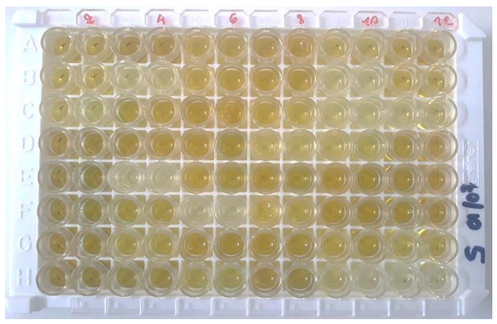

	PBS	RBD	PBS	RBD	PBS	RBD	PBS	RBD	PBS	RBD	PBS	RBD
A	G2	G2	H4	H4	D6	D6	D7	D7	D9	D9	A11	A11
B	H2	H2	B5	B5	E6	E6	E7	E7	F9	F9	B11	B11
C	A4	A4	D5	D5	F6	F6	G7	G7	G9	G9	E11	E11
D	B4	B4	F5	F5	G6	G6	H7	H7	A10	A10	F11	F11
E	D4	D4	G5	G5	H6	H6	C8	C8	B10	B10	H11	H11
F	E4	E4	H5	H5	A7	A7	D8	D8	E10	E10	A12	A12
G	F4	F4	A6	A6	B7	B7	E8	E8	F10	F10	G12	G12
H	G4	G4	C6	C6	C7	C7	F8	F8	G10	G10	BLANK	BLANK

	1	2	3	4	5	6	7	8	9	10	11	12
A	9,999	3,329	9,999	9,999	3,27	9,999	9,999	9,999	1,894	1,816	9,999	9,999
B	2,648	2,051	0,485	0,524	2,838	9,999	9,999	9,999	0,476	0,403	2,495	2,753
C	1,553	0,94	9,999	9,999	9,999	9,999	3,253	2,818	0,716	0,569	0,539	0,81
D	9,999	9,999	9,999	9,999	9,999	9,999	1,366	1,093	1,332	1,728	9,999	9,999
E	9,999	9,999	0,362	0,363	9,999	9,999	9,999	9,999	9,999	9,999	9,999	9,999
F	9,999	9,999	9,999	9,999	0,384	0,348	2,713	2,172	9,999	9,999	9,999	9,999
G	9,999	9,999	2,517	2,657	9,999	9,999	9,999	9,999	2,265	9,999	1,71	2,454
H	9,999	9,999	9,999	9,999	2,324	2,419	9,999	9,999	1,026	0,377	0,342	0,398

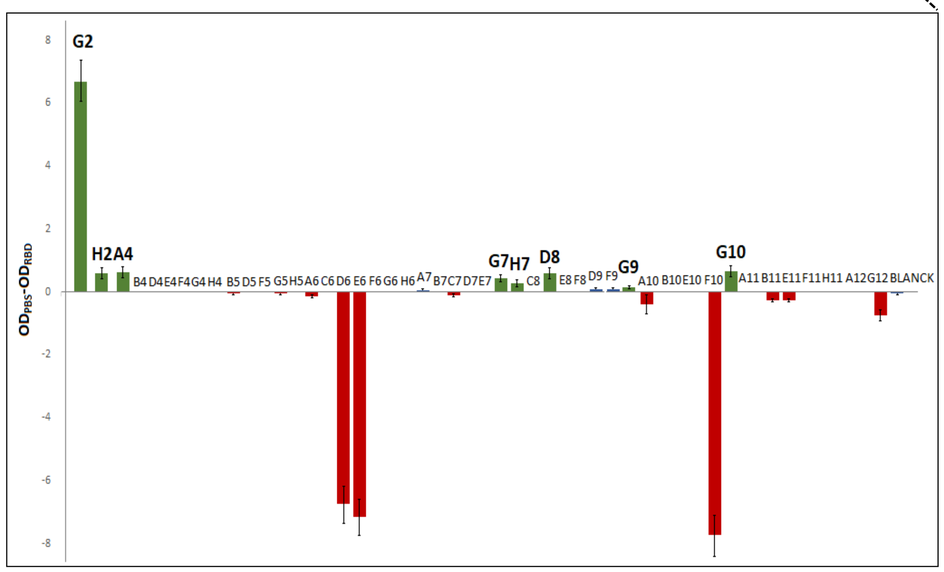

D.

DNA sequence of CDRs and FRs of Light chain
FR1:AACATTATGATGACACAGTCGCCATCATCTCTGGCTGTGTCTGCAGGAGAAAAGGTCACTATGAGCTGTAAGTCCAGTT
CDR1:CAAAGTGTTTTATACAGTTCAAATCAGAAGAACTAC
FR2:TTGGCCTGGTACCAGCAGAAACCAGGGCAGTCTCCTAAACTGCTGATCTAC
CDR2:TGGGCATCC
FR3:ACTAGGGAATCTGGTGTCCCTGATCGCTTCACAGGCAGTGGATCTGGGACAGATTTTACTCTTACCATCAGCAGTGTACAAGCTGAAGACCTGGCAGTTTATAC
CDR3:TGTCATCAATACCTCTCCTCGCTCACGTTC

DNA sequence of CDRs and FRs of Heavy chain
FR1:GAAGTGATGCTGGTGGAGTCTGGGGGAGGCTTAGTGAGGCCTGGAGGGACCCTGAAACTCTCCTGTGCAGCCTCT
CDR1:GGATTCACTTTTAGTGACGCCTGG
FR2:ATGGACTGGGTCCGCCAGTCTCCAGAGAAGGGGCTTGAGTGGGTTGCTGAA
CDR2: ATTAGAAACAAAGCTAATAATCATGCAACA
FR3:TACTATGCTGAGTCTGTGAAAGGGAGGTTCACCATCTCAAGAGATGATTCCAAAAGTAGTGTCTACCTGCAAATGAACAACTTAAGAGCTGAAGACACTGGCATTTATTAC
CDR3:TGTACCAGGCTCTATTACTACGGTAGTACCTACTACTTTGACTACTG
FR4:GGCCAAGGCACCACTCTCACAGTCTCCTCAG

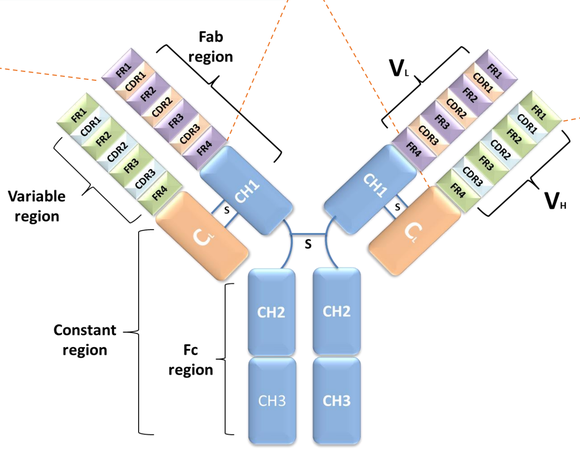

Figure S2

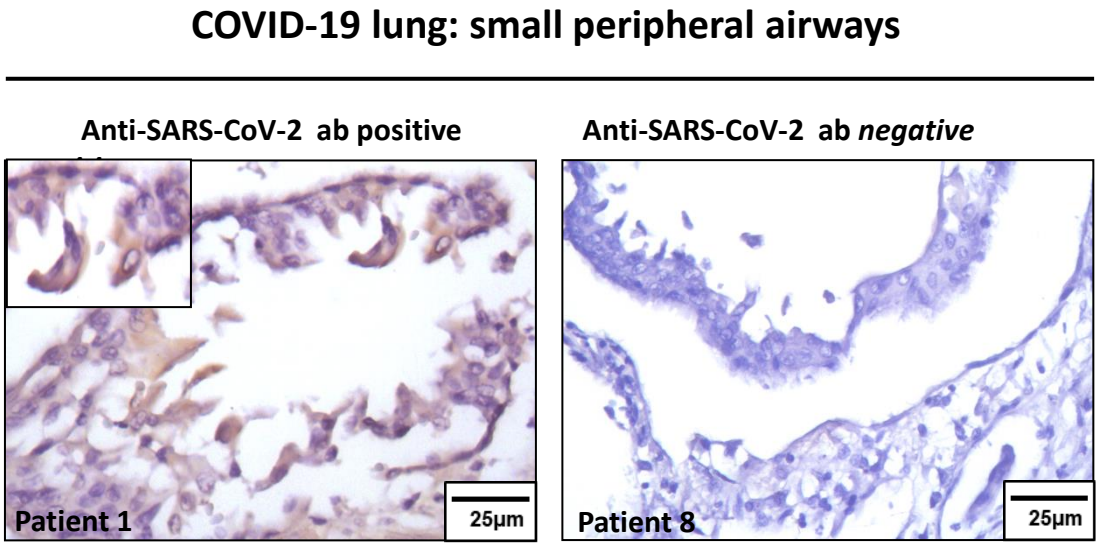
COVID-19 lung: small peripheral airways
Anti-SARS-CoV-2 ab positive
Anti-SARS-CoV-2 ab *negative*
Patient 1
25µm
Patient 8
25µm

Figure S3

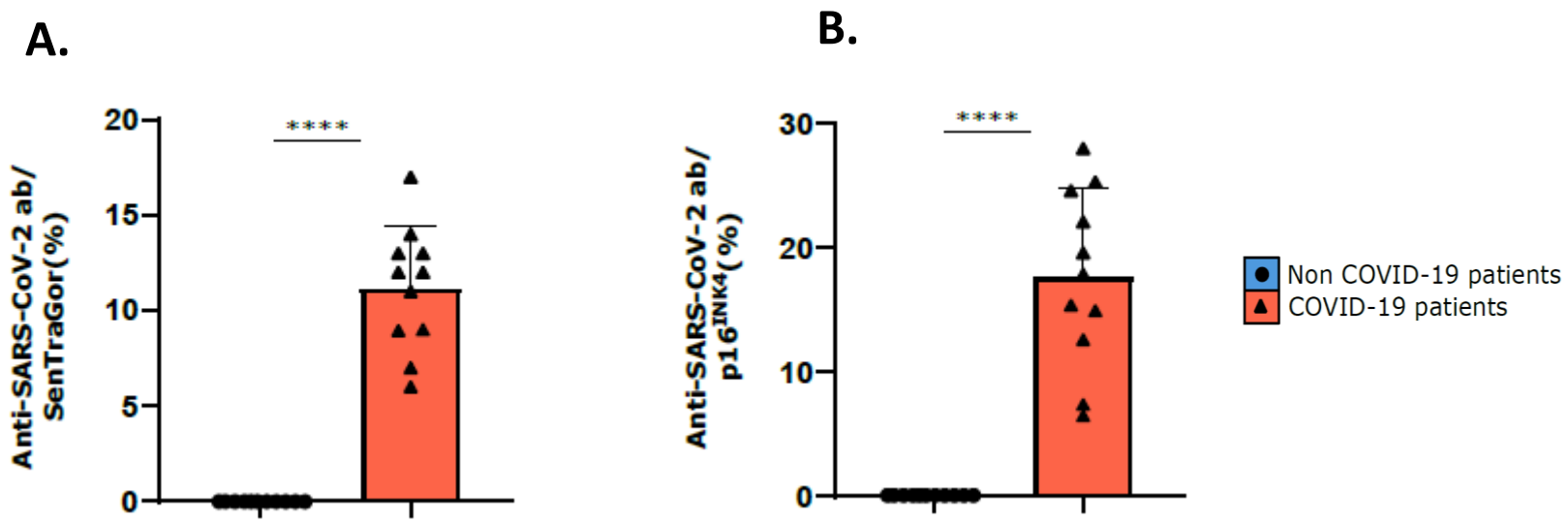
A.
B.
Anti-SARS-CoV-2 ab/ SenTraGor(%)
Anti-SARS-CoV-2 ab/ p16INK4(%)
****
****
20
15
10
5
0
30
20
10
0
Non COVID-19 patients
COVID-19 patients

Figure S4

A. Non COVID-19 Lung (Acute pneumonia)

Anti-SARS-CoV-2 ab

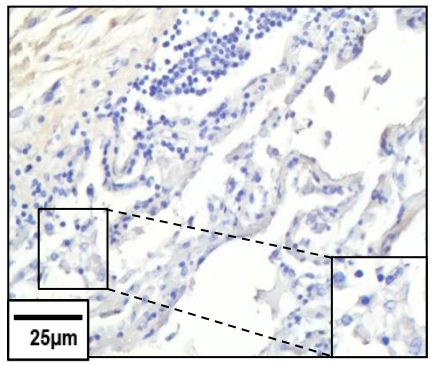

Anti-SARS-CoV-2 ab

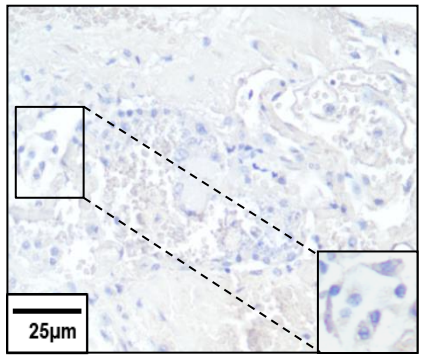

SenTraGor

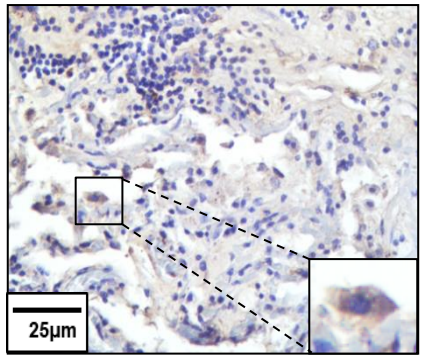

SenTraGor

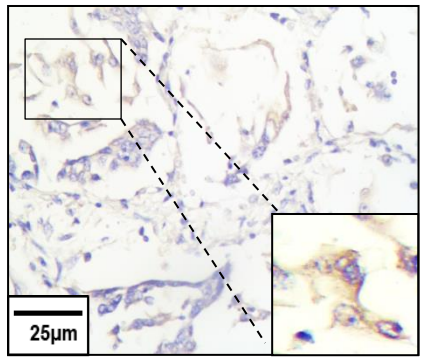

p16^{INK4a}

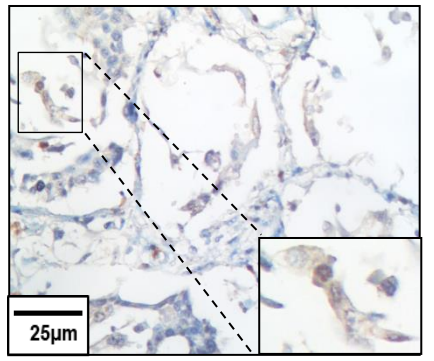

ACE-2

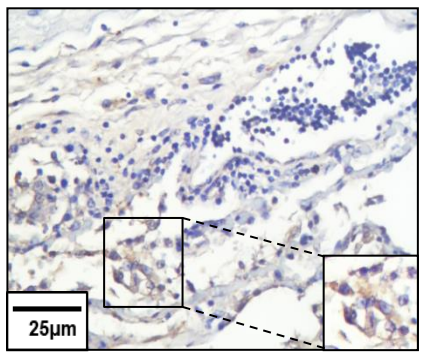

TTF-1

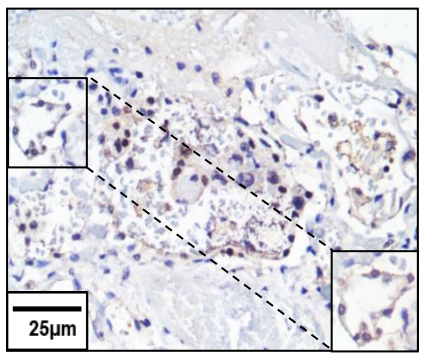

IL-6

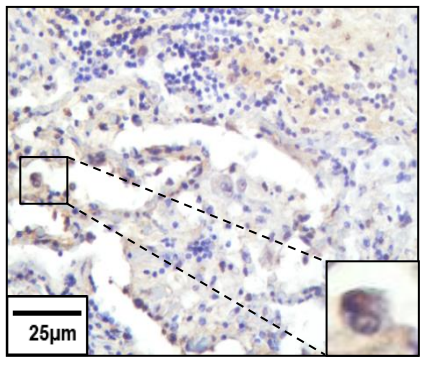

SenTraGor

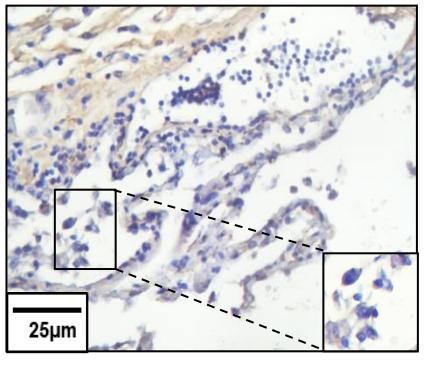

SenTraGor

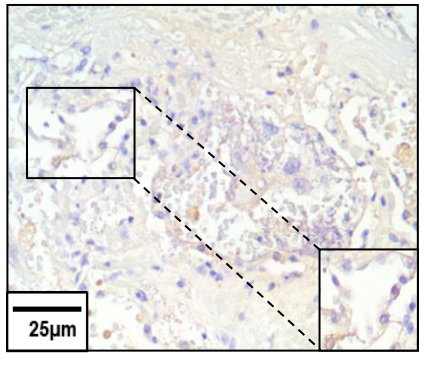

IL-1β

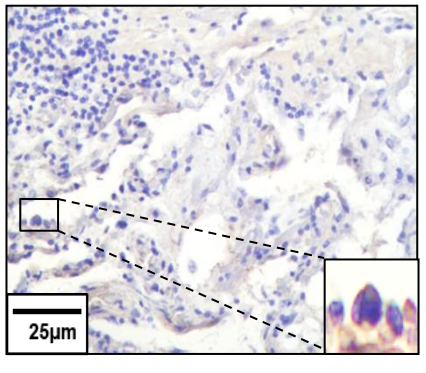

B.

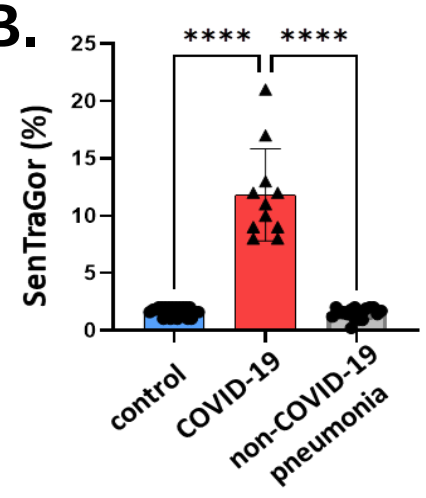

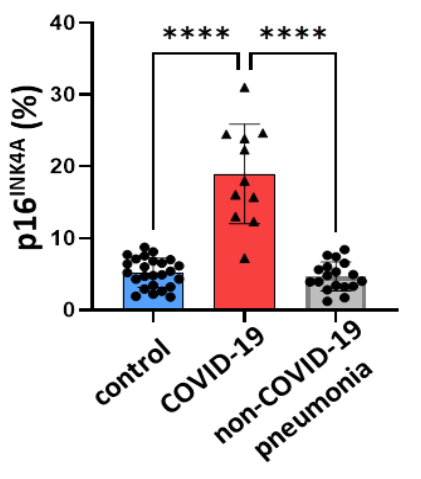

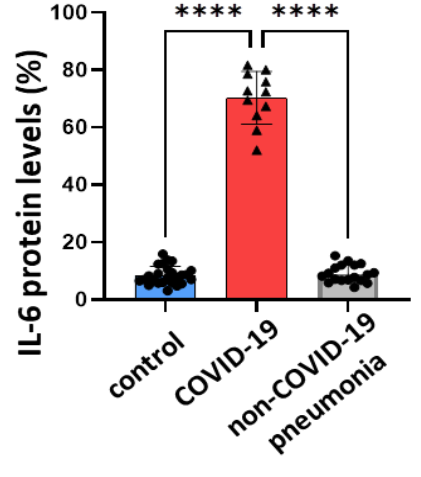

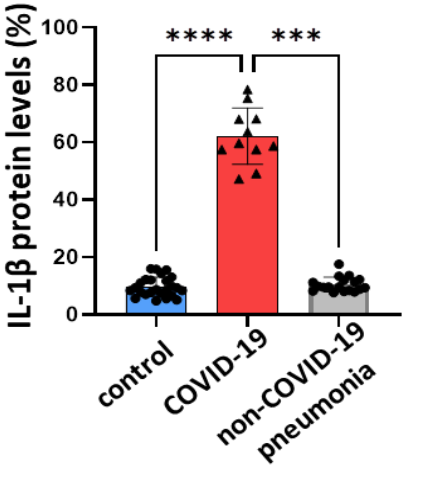

Figure S5

A. Vero cells (Double staining analysis)

1. SARS-CoV-2/ SENESCENCE

2. PROLIFERATION/SENESCENCE

3. SENESCENCE

UNINFECTED

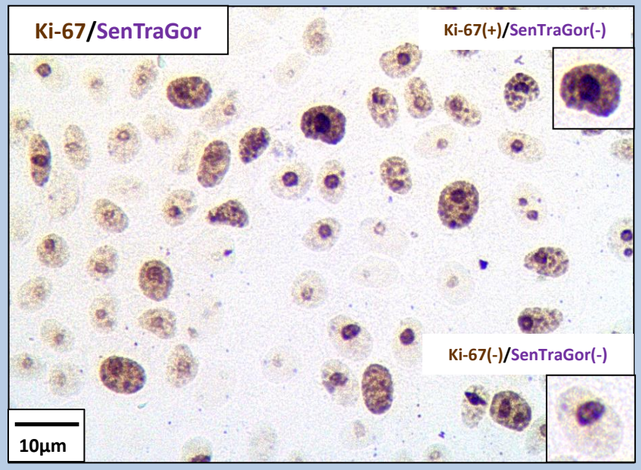

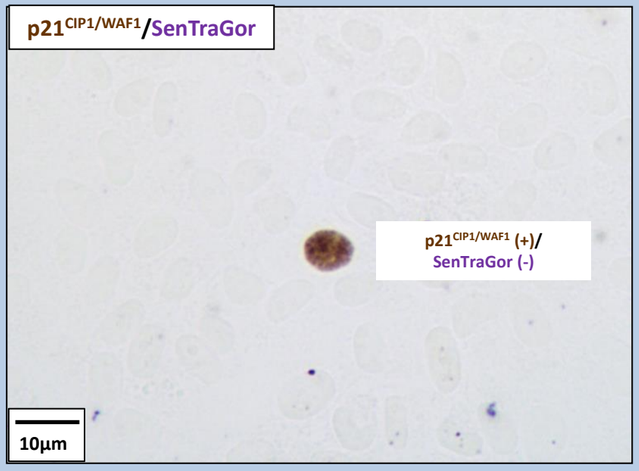

SARS-CoV-2 INFECTED (with strain B.1.222)

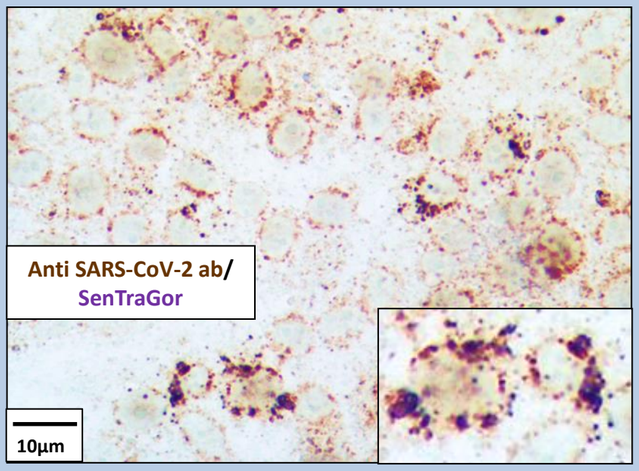

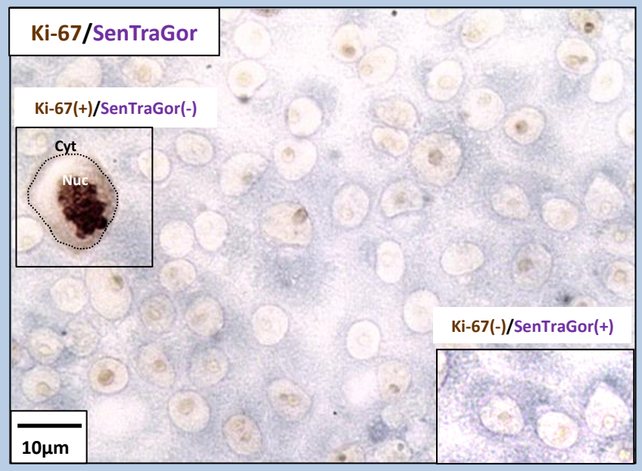

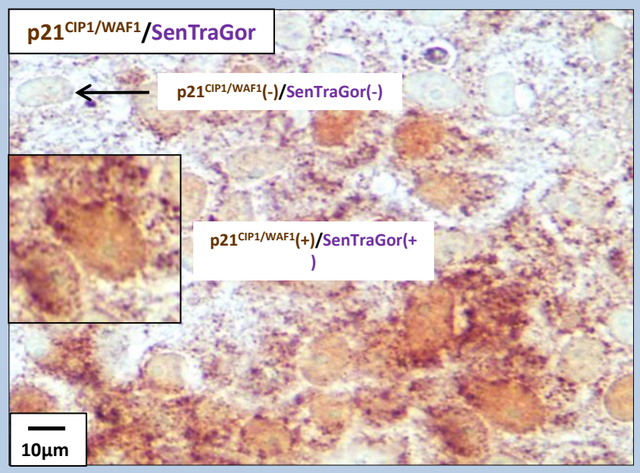

B. Alveospheres

UNINFECTED

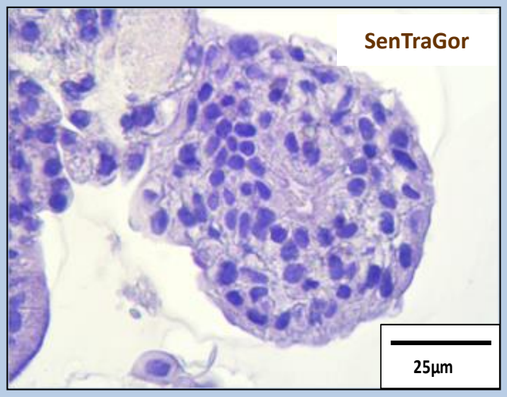

SENESCENCE (-)

SARS-CoV-2 INFECTED

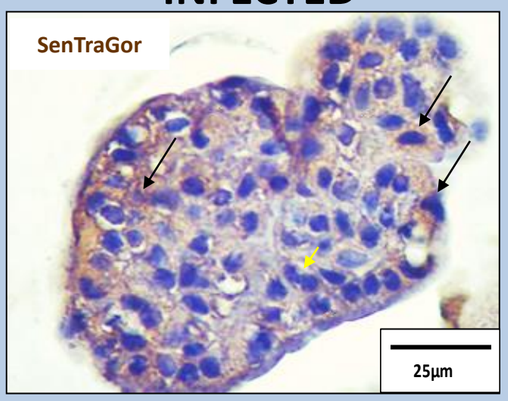

SENESCENCE (+)

Figure S6

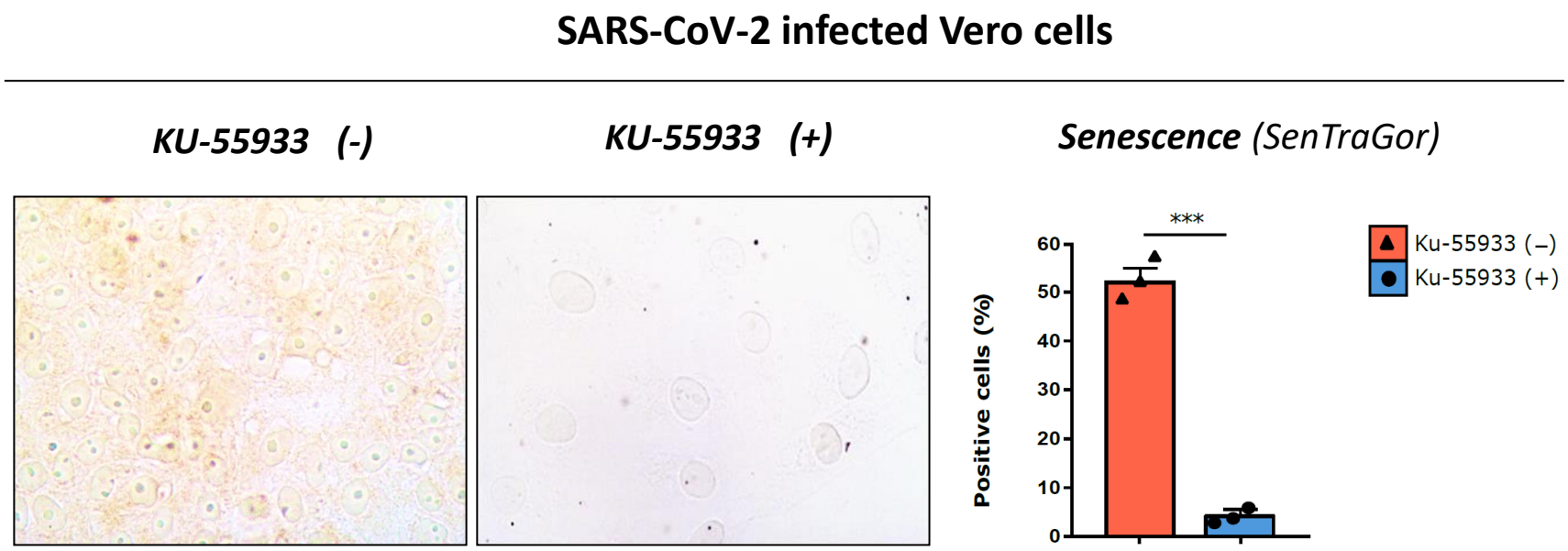
SARS-CoV-2 infected Vero cells
KU-55933 (-)
KU-55933 (+)
Senescence (SenTraGor)
***
Positive cells (%)
60
50
40
30
20
10
0
Ku-55933 (–)
Ku-55933 (+)

Figure S7

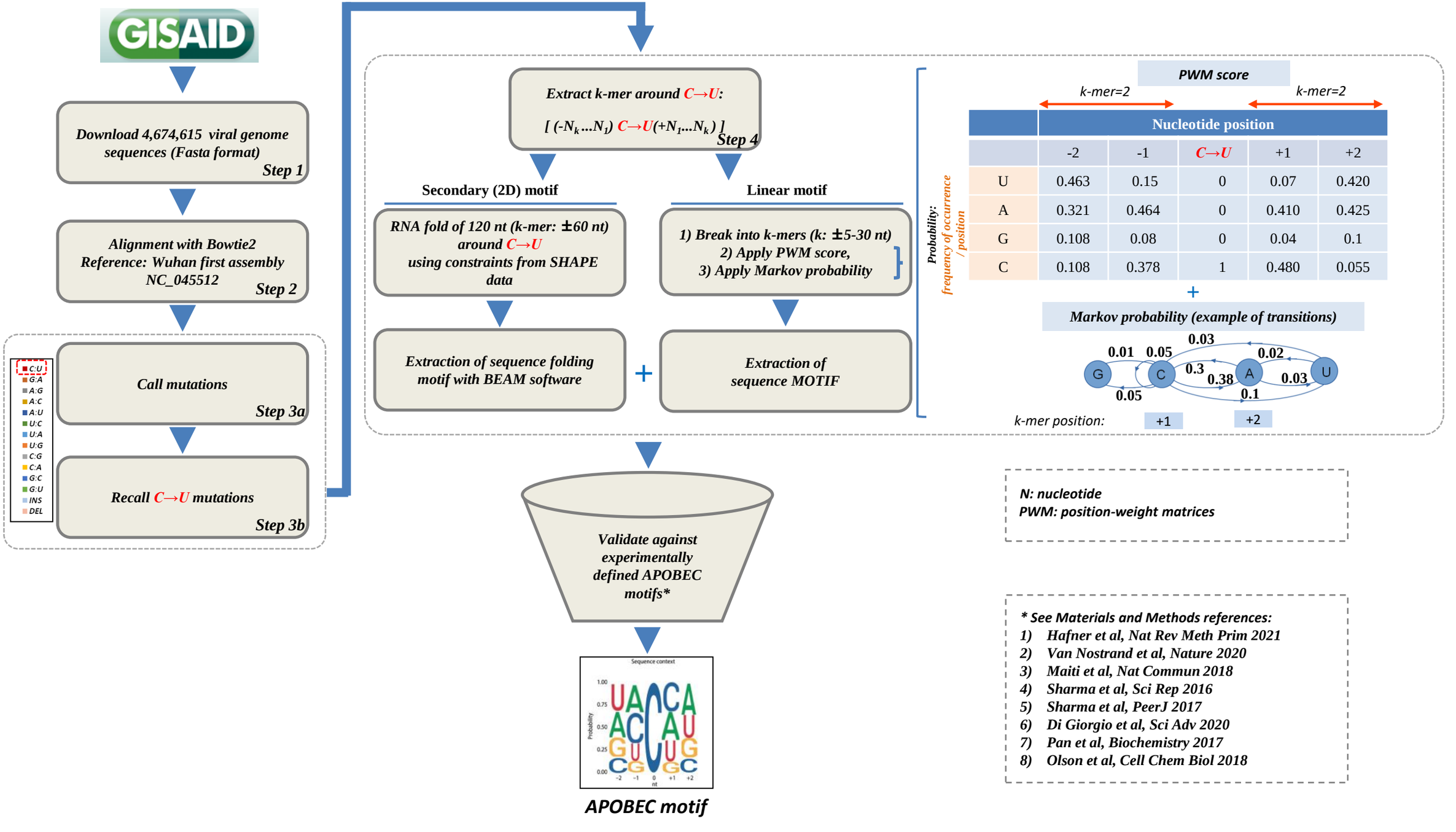
GISAID
Download 4,674,615 viral genome sequences (Fasta format)
Step 1
Alignment with Bowtie2
Reference: Wuhan first assembly NC_045512
Step 2
C:U
G:A
A:G
A:C
A:U
U:C
U:A
U:G
C:G
C:A
G:C
G:U
INS
DEL
Call mutations
Step 3a
Recall C→U mutations
Step 3b
Extract k-mer around C→U:
[(-Nk ...N1) C→U(+N1...Nk)]
Step 4
Secondary (2D) motif
Linear motif
RNA fold of 120 nt (k-mer: ±60 nt) around C→U using constraints from SHAPE data
1) Break into k-mers (k: ±5-30 nt)
2) Apply PWM score,
3) Apply Markov probability
Extraction of sequence folding motif with BEAM software
+
Extraction of sequence MOTIF
Probability: frequency of occurrence / position
PWM score
k-mer=2
k-mer=2
Nucleotide position
-2 -1 C→U +1 +2
U 0.463 0.15 0 0.07 0.420
A 0.321 0.464 0 0.410 0.425
G 0.108 0.08 0 0.04 0.1
C 0.108 0.378 1 0.480 0.055
+
Markov probability (example of transitions)
G C A U
0.01 0.05 0.03 0.02 0.3 0.38 0.03 0.05 0.1
k-mer position: +1 +2
Validate against experimentally defined APOBEC motifs*
Sequence context
Probability
nt
APOBEC motif
N: nucleotide
PWM: position-weight matrices
* See Materials and Methods references:
1) Hafner et al, Nat Rev Meth Prim 2021
2) Van Nostrand et al, Nature 2020
3) Maiti et al, Nat Commun 2018
4) Sharma et al, Sci Rep 2016
5) Sharma et al, PeerJ 2017
6) Di Giorgio et al, Sci Adv 2020
7) Pan et al, Biochemistry 2017
8) Olson et al, Cell Chem Biol 2018

Figure S8

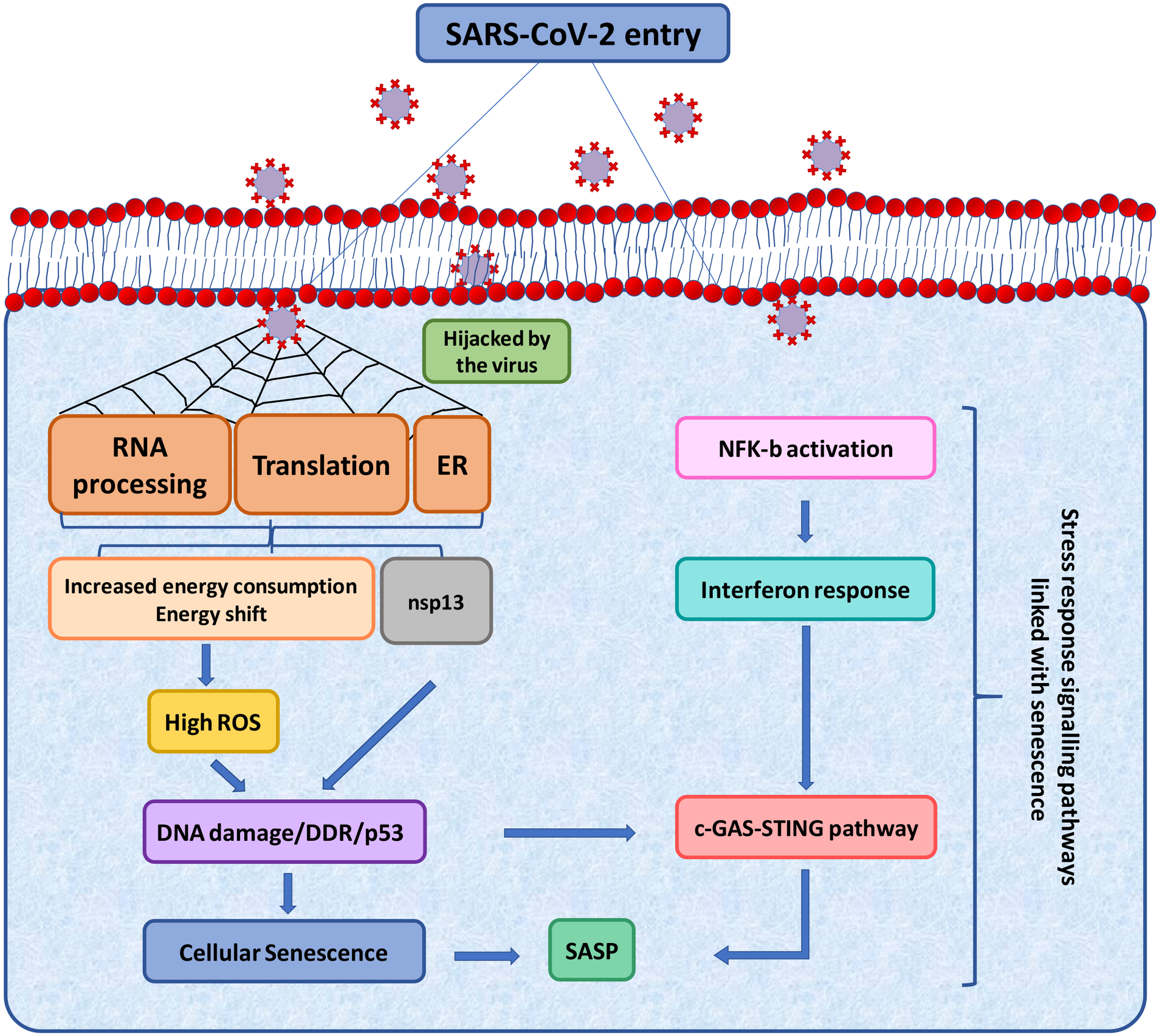

Abbreviations. SARS-CoV-2: Severe acute respiratory syndrome coronavirus 2; ER: endoplasmic reticulum; ROS: Reactive Oxygen Species; DDR: DNA Damage Response; SASP: senescence-associated secretory phenotype.

References

- Hekman et al, Mol Cell 2020
- Lee et al, Nature 2021
- Victor et al, Biochem Biophys Res Com 2021
- Bartkova et al, Nature 2006
- Gorgoulis et al, Cell 2019

Figure S9

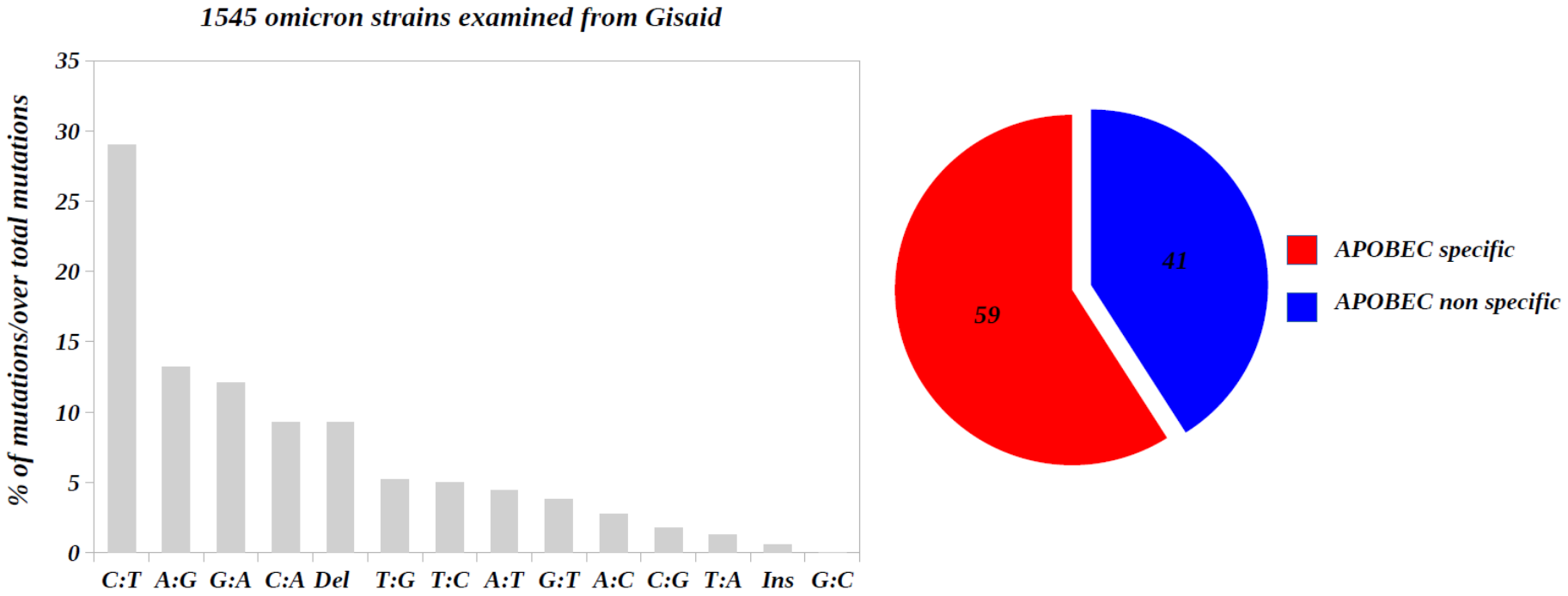
1545 omicron strains examined from Gisaid
% of mutations/over total mutations
35
30
25
20
15
10
5
0
C:T
A:G
G:A
C:A
Del
T:G
T:C
A:T
G:T
A:C
C:G
T:A
Ins
G:C
59
41
APOBEC specific
APOBEC non specific

Figure S10

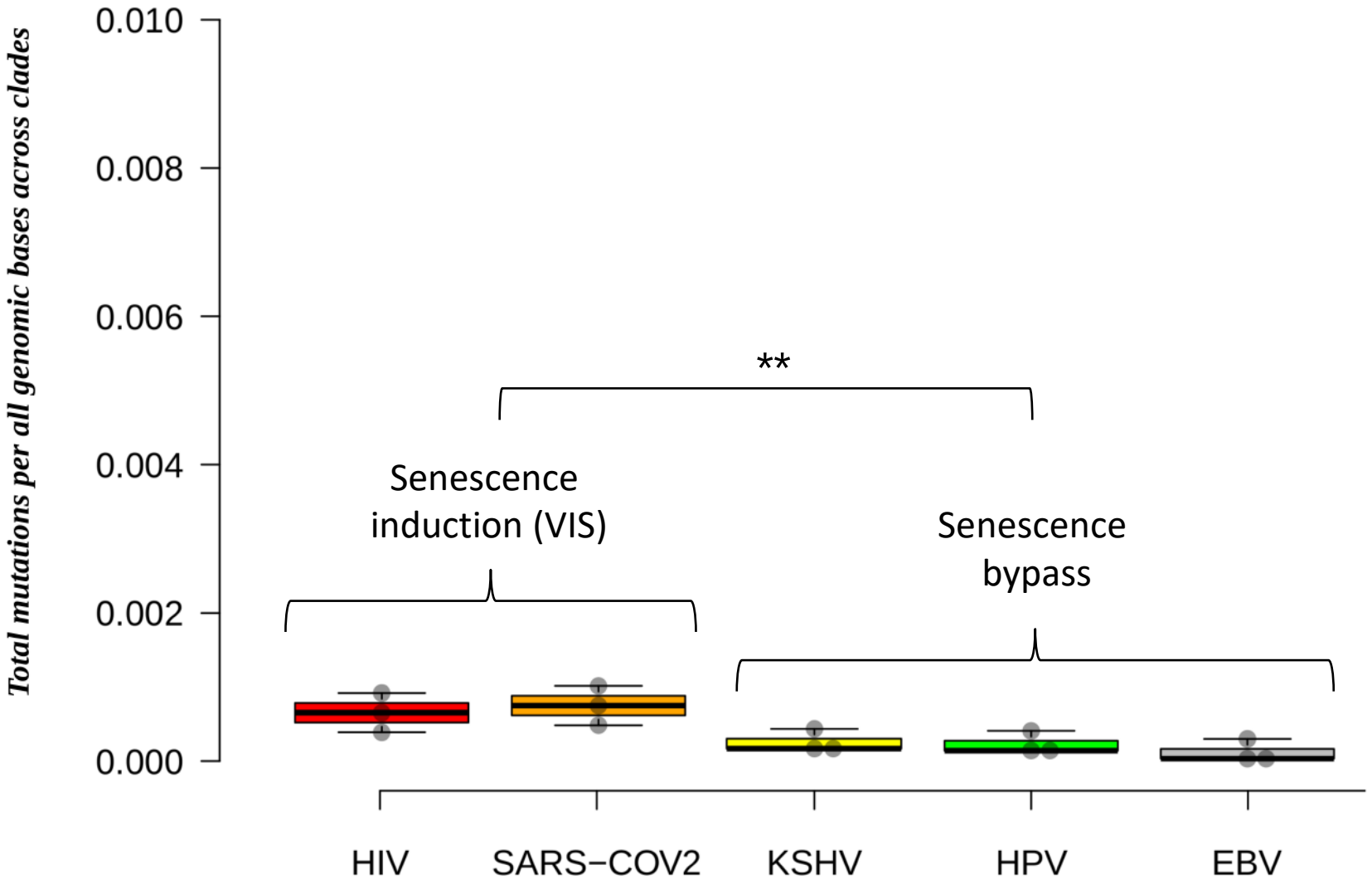
Total mutations per all genomic bases across clades
0.010
0.008
0.006
0.004
0.002
0.000
**
Senescence induction (VIS)
Senescence bypass
HIV
SARS−COV2
KSHV
HPV
EBV

SUPPL TABLE 1: CLINICOPATHOLOGICAL CHARACTERISTICS OF COVID AND NON COVID-19 CASES

Suppl Table 1A: Clinicopathological characteristics of COVID-19 cases examined along with G2 antibody, anti-S antibody (GENETEK), senescence, IL-6 and IL-1β evaluation results in the corresponding lung tissues

CASE	SEX	AGE	DATE OF DEATH	DATE OF COVID-19 TEST	HOSPITALIZED DAYS	DAYS IN INTENSIVE CARE UNIT	RESPIRATORY ASSISTANCE	TREATMENTS	COMORBIDITIES	MOLECULAR TEST	G2 EVALUATION		COMERCIAL ANTI-S AB (GENETEK) EVALUATION		SenTraGor EVALUATION (%)	P16 (%)	IL-6 (%)	IL-1b (%)
											Schaefer et al, 20120	Remmelink et al, 2020	Schaefer et al, 20120	Remmelink et al, 2020				
A2000026	F	73	05/03/2020	01/03/2020	4	-	NO	Kaletra, Remdesevir	Follicular lymphoma grade 1-2. Mixed type cardiopathy on chemotherapy	Positive	<5/4 mm² (+)	++	<5/4 mm² (+)	++	9	12.3	80	57.42
A2000036	M	87	20/03/2020	16/03/2020	5	4	YES	Reyataz,Co-amoxiciline	Type 2 non-insulin dependent diabetes. Dyslipidemia	Positive	>5-50/4 mm² (+++)	+++	>5-50/4 mm² (+++)	+++	17	24.47	52	59.65
A2000038	F	74	21/03/2020	12/03/2020	9	5	YES	Pipéracilline + tazobactam Atanazavir + hydroxychloroquine Remdesevir	COPD stage IIb. Pacemacer for rhythmic cardiopathy. Non-smoker	Positive	5-50/4 mm² (++)	+++	5-50/4 mm² (++)	+++	12	15.71	72.72	68.12
A2000042	M	80	28/03/2020	16/03/2020	13	13	YES	Augmentin+ventolin Tazobactam Plaquénil + Reyataz	COPD stage II	Positive	5-50/4 mm² (++)	+++	5-50/4 mm² (++)	+++	13	22.32	69.47	75.32
A2000045	M	96	01/04/2020	24/03/2020	8	8	NO	Co-amoxicilline Procalcitonine Hydroxychloroquine	Chronic renal failure. Pulmonary embolism (2019).	Positive	<5/4 mm² (+)	++	<5/4 mm² (+)	++	10	17.97	81.62	68
A2000047	M	75	02/04/2020	10/03/2020	7	7	YES		Hypertrophic cardiomyopathy. Pacemaker for complete atrioventricular block. Type 2 non-insulin dependent diabetes. Overweight.	Positive	5-50/4 mm² (++)	+++	5-50/4 mm² (++)	+++	11	24.66	67.3	47.22
A2000048	M	36	02/04/2020	01/04/2020	2	2	YES		Tetraplegia. Post-anoxic encephalopathy. Aspiration pneumonia	Weakly positive	<5/4 mm² (+)	++	<5/4 mm² (+)	++	9	16.04	64.14	49.1
A2000052	M	61	16/04/2020	01/04/2020	18	18	YES	Vancomycine + rifampicine Imipénème Noradrénaline	Ischemic heart disease. Hypertension. Type 2 non-insulin dependent diabetes. Peripheral artery disease (PAD). COPD with asthmatic component. Alcohol dependent syndrome. Possible hemochromatosis.	Weakly positive	<5/4 mm² (+)	++	<5/4 mm² (+)	++	8	23.87	78.55	63.67
A2000058	F	72	27/04/2020	26/04/2020	4	4	NO	Co-amoxicilline Pipéracilline – Tazobactam Furosémide	Hypertension. Chronic renal failure. COPD, former smoker. Bipolar disorder under long-term lithium treatment. Peripheral artery disease (PAD)	Positive	5-50/4 mm² (++)	+++	5-50/4 mm² (++)	+++	12	13	72.36	78.4
A2000062	M	70	07/05/2020	n.c.	34	26	YES	Co-amoxicilline Hydrochloroquine Céfépime Dobutamine Pipéracilline-Tazobactam Méropénème Lévosimendan Aspirine et Clopidogrel Levetiracetam Pipéracilline-Tazobactam et Vancomicine	Ischemic and valvular heart disease. Hypertension.	Weakly positive	<5/4 mm² (+)	++	<5/4 mm² (+)	++	8	7.2	58.96	57.43
3403/20 B2	M	56	11/12/2020	02/12/2020	10	6	YES	Dexamethasone, Pregabalin, Insulin therapy, Piperacillin-Tazobactam, Vancomycin, Azithromycin	Decompensated Liver Cirrhosis, Hemophilia A, Type 2 Diabetes, Brain mass under investigation	Positive	>5-50/4 mm² (+++)	+++	>5-50/4 mm² (+++)	+++	21	31	75.9	58.72

SUPPL TABLE 1: CLINICOPATHOLOGICAL CHARACTERISTICS OF COVID AND NON COVID-19 CASES

Suppl Table 1B: Clinicopathological characteristics of non COVID-19 cases examined along with senescence, IL-6 and IL-1β evaluation results in the corresponding lung tissues

CASE	SEX	AGE	SMOKING	HISTOLOGY	GRADE	T	N	M	STAGE	COMORBIDITIES	SenTraGor EVALUATION (%)	P16 (%)	IL-6 (%)	IL-1b (%)
K14	F	72	M	1	3	1	0	0	IA		1	3.2	8.52	9.36
K22	M	84	H	1	2	2	0	0	IB	COPD	2	4.7	13.47	15.78
D30	F	76	H	1	3	2	0	0	IB	COPD	2	5.2	5.78	7.36
D8	M	80	H	1	3	3	2	0	IIIA		2	7.1	7	5.14
D19	M	84	M	2	3	2	0	0	IB	COPD	1.6	1.93	15.87	14.36
D23	M	76	M	1	2	1	1	0	IIA	Hypertension, Diabetes	1	8.74	10.63	12
A23	M	42	M	1	3	2	2	0	IIIA		2	4.31	9.4	11.68
D52	M	61	H	2	3	2	0	0	IIA	Coronary artery disease, COPD	1.8	6.14	12.36	15.92
K53	F	72	H	5	2	1	0	0	IA		1	4.92	6.87	9.87
K50	M	70	M	2	2	1	1	0	NA	Hypertension	1.8	7.55	4.82	7.84
K42	M	57	H	2	3	2	0	0	IB	COPD	2	6	8.7	8.7
K38	F	44	M	1	3	2	0	0	IB	Hypertension	1.6	7.7	7.6	8.5
B12	M	66	H	2	3	2	0	0	IB	Coronary artery disease, COPD	2	4.3	3.1	5.6
K41	M	69	H	1	2	2	1	0	IIB	Hypertension, Diabetes	1.8	2.6	12.54	11
D27	M	43	M	2	2	2	0	0	IB		1	6.8	5.9	8.4
D13	M	77	H	5	4	2	0	0	IB	COPD	2	2.2	6	4.8
D36	M	80	H	2	2	2	0	0	IB	Coronary artery disease, COPD	2	5.4	13.8	9.36
K26	F	79	H	1	2	1	0	0	IA	COPD	1.6	1.8	6.5	5.5
D35	M	73	H	1	3	2	0	0	IB		1.6	6.4	5	7.7
K19	F	69	M	2	3	2	1	0	IIB	COPD	1.6	7	7.8	12.2
D28	M	76	H	2	2	2	1	0	IIB	COPD	1.6	8.1	10.14	8.4
D20	M	75	H	1	3	1	1	0	IIA	Coronary artery disease, COPD	1.8	3.4	8.3	7
D44	F	63	M	2	3	2	0	0	IB		1	2.9	5.5	6.6
B10	M	77	H	1	2	2	1	0	IIB	COPD	2	4.8	9	15.52
K19	F	78	M	2	3	2	1	0	IIB	Coronary artery disease, COPD	2	6.5	7	13
AP1	M	70	H	6						Stroke, Hypertension, Diabetes	1	4.95	8.7	9.36
AP2	M	77	H	6						Stroke, Hypertension, Diabetes	2	6	9.4	12.2
AP3	M	84	H	6						Stroke, Cardiac and renal failure	1.6	7.6	12	11.4
AP4	F	81	H	6						Stroke, Coronary artery disease	2	8.4	13.5	11.92
AP5	M	71	H	6						Stroke, Diabetes	1.2	5.6	7.80	9.60
AP6	M	69	H	6						Stroke	0.9	7.43	12.50	9.50
AP7	F	74	H	6						Stroke, Diabetes	0.2	3.4	4.30	8.00
AP8	F	79	M	6						Stroke, Coronary artery disease	2	6.5	6.90	11.20
AP9	M	83	M	6						Stroke, Cardiac failure, Anemia	1.4	1.2	8.20	13.40
AP10	M	84	H	6						Stroke, Cardiac failure	1.6	3.9	5.70	8.40
AP11	M	72	M	6						Stroke, Coronary artery disease, Lupus	1.9	4	11.00	9.90
AP12	F	77	H	6						Stroke, Coronary artery disease	1.8	5.3	15.30	17.50
AP13	F	63	H	6						Stroke, Coronary artery disease, Diabetes	1.5	3.3	6.70	7.60
AP14	M	83	M	6						Stroke, Hypertension, Diabetes	0.9	1.7	7.10	8.20
AP15	F	76	M	6						Stroke, Coronary artery disease, Diabetes	1.4	2.8	9.20	9.60
AP16	F	67	H	6						Stroke, Coronary artery disease	1.7	3.9	6.70	8.80
AP17	F	79	H	6						Stroke, Diabetes, Cardiac failure	1.6	4.8	5.90	7.90
AP18	M	70	M	6						Stroke, Coronary artery disease	2	3.2	12.00	13.60

SUPPL TABLE 1: CLINICOPATHOLOGICAL CHARACTERISTICS OF COVID AND NON COVID-19 CASES

Smoking	Medium: 30-50 cigarretes/day
	Heavy: > 50 cigarettes/day
Histology	1. Squamous carcinoma
	2. Adenocarcinoma
	3. Large Cell carcinoma
	4. Undifferentiated carcinoma
	5. Other carcinoma type
	6. Acute (aspiration) pneumonia
	NA. non-available